J. Fluid Mech. (1995), vol. 286, pp. 173–200

Surface-tension-driven flows at low Reynolds number arising in optoelectronic technology

By A. L. YARIN

Faculty of Mechanical Engineering, Technion-Israel Institute of Technology, Haifa 32000, Israel

(Received 14 February 1994 and in revised form 10 October 1994)

Some methods of formation of preforms for drawing of polarization-maintaining optical fibres are based on utilization of the surface tension of glass in the liquid state. Under the action of surface tension non-circular glass articles begin to flow, which results in formation of an anisotropic internal structure of the preforms. The hydrodynamic analysis of two such methods is given in the paper. Analytical solutions of the Stokes equations with linearized boundary conditions for the corresponding creeping surface-tension-driven flows of liquid glass are obtained. By means of these solutions a processing strategy may be predetermined with a view to a specific internal structure of the fibre, as well as to the required value of birefringence. The theoretical results are compared with experimental data and agreement is fairly good.

1. Introduction

The polishing method used for creation of preforms for drawing of polarization-maintaining optical fibres is based on the following principles (Kaminow *et al.* 1979). The initial cross-section of a glass preform is shown in figure 1, where the domain 0 corresponds to the core through which a signal propagates, domain 1 to the cladding which serves to impose stresses on the core, and domain 2 to the outer matrix of the preform (as well as the fibre which will be drawn from it).

The material (glass) of the core differs in composition and in physical properties from those of the cladding and outer matrix. In its turn, the material (glass) of the cladding differs from that of the outer matrix.

A part of the outer matrix is removed (polished) – as shown by the dashed lines in figure 1, for example – and the preform is placed in a furnace and heated until the cladding and outer matrix soften. The core remains hard. Surface tension at the boundary Γ_2 begins to round it off. The resulting flow of molten glass deforms the boundary Γ_1 subjected to the interfacial tension which is lower than the surface tension at the boundary Γ_2. Deformation of the boundary Γ_1 causes it to lose its circular form. Meanwhile, the boundary Γ_0 remains unchanged since the core continues to be hard. Note that the case of a negligibly small core (effectively, a two-layer preform) is also of interest.

Cooling and solidifying of the preform at some intermediate moment of time yields a hard preform with a non-circular cladding boundary Γ_1, whereas the outer boundary Γ_2 is already practically circular (the boundary Γ_0 is always circular). It is emphasized that duration of the heat treatment should not be very long, since in the end the boundary Γ_1 will also begin to approach a circle if the interfacial tension is non-zero.

Owing to the difference in the thermoelastic properties of the materials in the cladding and outer matrix, an anisotropic field of elastic stresses is created in the hard

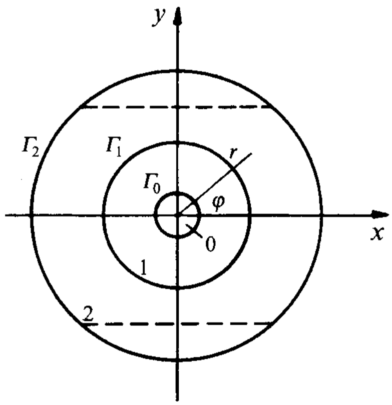

FIGURE 1. Initial configuration in the cross-section of the preform. 0 is the core, where a signal propagates; 1 is the stress cladding; 2 is the outer matrix. Γ_0 is the boundary between the core and cladding; Γ_1 is the boundary between the cladding and outer matrix; Γ_2 is the outer boundary of the cross-section.

preform cross-section (as well as in the optical fibre drawn from it) which results in birefringence. Accordingly, the core becomes capable of transmitting signals with a certain polarization.

Although the above-mentioned method is used extensively, there is no quantitative theory that permits one to predict what shape the cladding will have for a given initial shape of the outer surface of the matrix and material parameters of the preform. A solution of this problem for three- and two-layer preforms is one of the main objectives of the present paper. We also address the inverse problem – prediction of the polished shape of the outer matrix needed in order to arrive at the prescribed shape of the cladding.

The second method of preform creation employs a modified chemical vapour deposition process (MCVD; Kaminow 1981) or a non-symmetric one (N-MCVD; Doupovec & Yarin 1991). In these techniques glass particles are thermophoretically deposited from a gas flow onto the inner surface of a glass substrate tube, creating a coating. Afterwards the tube is heated, softens and begins to collapse. The latter means that creeping flow of highly viscous liquid (glass) directed towards the centre arises under the action of surface tension, which tends to reduce the free surface area, filling up the cavity with the material. Thus, the slow viscous flow of the glass is driven by surface tension and (perhaps) a pressure differential between the inner and outer tube surfaces (Geyling, Walker & Csentits 1983).

The aim of the present work is to describe analytically the collapse of the substrate tube with radially non-symmetric layers inside. The simplest model system with a single-layer coating shown in figure 2 is considered. Note that previous publications on the collapse of viscous tubes treated only the axisymmetric case (Lewis 1977, where the interfacial tension was taken to be zero and pressure difference was accounted for; Das & Gandhi 1986, where the interfacial tension was also taken to be zero and viscosity/temperature dependence was accounted for).

With the system shown in figure 2 collapsed, solidification results in a two-layer non-symmetric preform (the case of a negligibly small core), which possesses birefringence and polarization-maintaining properties for the same reasons as in the polishing method – owing to the difference in the thermoelastic properties of the materials.

The plan of the paper is as follows. In §2 we quote some typical numbers for

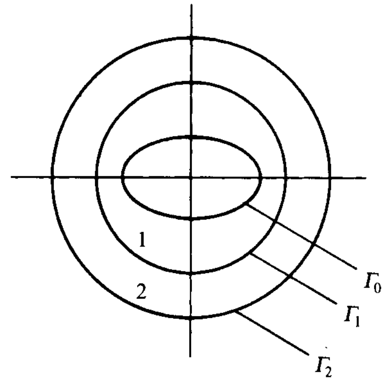

FIGURE 2. Single-layer coating in the tube collapse process. Layers 1 and 2 represent deposited domain and substrate tube material domain, respectively. Boundaries Γ_0, Γ_1 and Γ_2 denote the inner, the median and the outer interfaces, respectively.

dimensions and properties of the preforms and timescales of the polishing method, and prove that the quasi-steady isothermal creeping flow is a valid approximation. Then also in §2 we obtain the linearized analytical solution for the flow arising in the polishing method in the general case of a three-layer preform. In §3 we obtain the linearized analytical solution for the surface-tension-driven collapse of non-symmetric composite tubes. The calculation results obtained for polishing of two- and three-layer preforms are presented in §4.1 where comparison with experimental data and a discussion are given. The results obtained for the collapse method are shown and discussed in §4.2. In conclusion, in §5 we summarize the results.

2. Creeping flow in the polishing method

In the polishing method a preform is heated in a furnace by a convective medium at distant temperature T_∞. A reasonable value of the heat transfer coefficient $h = 1.5 \times 10^2$ W m^{-2} °C^{-1} (Paek & Runk 1978). Taking the radius of the unpolished outer matrix $R_2 = 0.6 \times 10^{-2}$ m and thermal conductivity of glass $k = 0.3 \times 10^2$ W m^{-1} °C^{-1} (Paek & Runk 1978), we obtain the reciprocal Biot number $Bi^{-1} = k/(hR_2) = 33.3$. A relationship of the temperature at any radius in a cylinder and the temperature on the centreline can be found from the known solution for conductive heat transfer or its graphic representation in the form of the Heisler chart (e.g. figure 4.11 in Bejan 1993). As a result, the temperature field in the cylinder is nearly homogeneous for $Bi^{-1} = 33.3$ during all the heating process, as is usually supposed for preforms and optical fibres (e.g. see Paek & Runk 1978).

However, the temperature of the cylinder changes with time. For $Bi^{-1} = 33.3$ it takes approximately time $t_0 = 40R_2^2/\alpha_T$ (α_T is the thermal diffusivity) to heat the cylinder to the temperature T_∞. Taking a glass density $\rho = 2.2 \times 10^3$ kg m^{-3} and specific heat $c_p = 1.05 \times 10^3$ J kg^{-1} °C^{-1}, as well as the above-mentioned value of k (Paek & Runk 1978), we obtain $\alpha_T = 0.13 \times 10^{-4}$ m^2 s^{-1} and $t_0 = 111$ s.

All the above estimates also hold for a polished preform.

The viscosity of glass fits the Arrhenius-type equation, $\mu = \mu_{i0} \exp(U_i/R_g T)$ over wide ranges of temperature (μ_{i0} and U_i are the pre-exponential factor and the viscous flow activation energy of a glass, respectively; R_g is the gas constant; T is the absolute temperature (Doremus 1973)). Molten glass is a highly viscous Newtonian liquid. If we take the temperature T_∞ corresponding to the working point of a glass T_w (at which the viscosity is $10^3\ \mathrm{kg\,m^{-1}\,s^{-1}}$), then isothermal flow (with $T = T_\infty$) resulting from the action of surface tension begins when $t_0 \approx 111$ s. The flow is negligible until the viscosity sharply decreases when temperature reaches $T \approx T_w$ (Doremus 1973). The value of the temperature T_∞ corresponding to the working point T_w (at which viscosity equals $10^3\ \mathrm{kg\,m^{-1}\,s^{-1}}$), typically ranges from 1800 to 2000 °C (Paek & Runk 1978; Oh 1979).

We can also take T_∞ higher than that corresponding to the working point T_w. Then temperature will continue to increase after flow has begun. However, temperature remains homogeneous over a cross-section of the preform. The viscosities of the glasses forming the cladding and outer matrix will change during such an overheat. If, however, the viscous flow activation energies are identical in the cladding and outer matrix (which is a realistic assumption for several pairs of glasses), $U_1 = U_2$, then according to the Arrhenius law given above, the viscosity ratio μ_1/μ_2 is temperature independent and thus, time independent – an important fact which is used below to generalize the solution obtained in the case of the polishing method with an overheat. (The subscripts 1 and 2 denote the activation energies and viscosities of the cladding and the outer matrix, respectively.)

It is emphasized that even in the worst case of $U_1 \neq U_2$ in an overheated preform, the situation may be considered approximately as an isothermal one, since the characteristic time of the temperature field saturation $\tau_1 = R_2^2/\alpha_T$ is small compared with the characteristic time of flow development, $\tau_2 = \mu R_2/\alpha_2$ (α_2 is the surface tension). Indeed, for $R_2 = 0.6\times10^{-2}$ m, $\alpha_T = 0.13\times10^{-4}\ \mathrm{m^2\,s^{-1}}$, $\mu \sim 10^3\ \mathrm{kg\,m^{-1}\,s^{-1}}$ and $\alpha_2 = 0.3\ \mathrm{kg\,s^{-2}}$ (Paek & Runk 1978), we obtain $\tau_1/\tau_2 = R_2\alpha_2/(\alpha_T\mu) = 0.138$.

Let us now estimate the Reynolds number characteristic of the polishing method. To this end we will prove that the flow is viscosity dominated. In the given surface-tension-driven flow the characteristic velocity is of the order of α_2/μ. Therefore, the Reynolds number $Re = \rho\alpha_2 R_2/\mu^2$ (which is also the reciprocal Ohnesorge number). To estimate the value of Re we take, as above, $\rho = 2.2\times10^3\ \mathrm{kg\,m^{-3}}$, $R_2 = 0.6\times10^{-2}$ m, $\mu = 10^3\ \mathrm{kg\,m^{-1}\,s^{-1}}$ corresponding to the working point, and $\alpha_2 = 0.3\ \mathrm{kg\,s^{-2}}$. As a result we obtain $Re = 3.96\times10^{-6}$. This Reynolds number is much less than unity and will remain much less than unity even when the preform is overheated (to prevent the onset of instabilities). The Reynolds number estimates the ratio of the inertial forces to the viscous ones. In the given problem additionally the ratio of the inertial term with time derivative in the Navier–Stokes equation to the viscous terms is also of the order of Re, since the characteristic time of the flow is $\mu R_2/\alpha_2$. Thus the viscous forces dominate all the inertial ones and the flow can be considered to be quasi-steady creeping flow (with boundary conditions which obviously are functions of time).

The creeping flow under consideration is planar, and its solution does not depend on the axial coordinate z. In polar coordinates r and φ (figure 1), we obtain the Stokes equations (Happel & Brenner 1965) in each of the domains 1 and 2 in the form

$$-\frac{\partial p}{\partial r}+\mu\left(\frac{\partial^2 v_r}{\partial r^2}+\frac{1}{r}\frac{\partial v_r}{\partial r}+\frac{1}{r^2}\frac{\partial^2 v_r}{\partial \varphi^2}-\frac{v_r}{r^2}-\frac{2}{r^2}\frac{\partial v_\varphi}{\partial \varphi}\right)=0, \tag{2.1a}$$

$$-\frac{1}{r}\frac{\partial p}{\partial \varphi}+\mu\left(\frac{\partial^2 v_\varphi}{\partial r^2}+\frac{1}{r}\frac{\partial v_\varphi}{\partial r}+\frac{1}{r^2}\frac{\partial^2 v_\varphi}{\partial \varphi^2}+\frac{2}{r^2}\frac{\partial v_r}{\partial \varphi}-\frac{v_\varphi}{r^2}\right)=0, \tag{2.1b}$$

$$\frac{\partial}{\partial r}(r v_r)+\frac{\partial v_\varphi}{\partial \varphi}=0, \quad v_z=0, \tag{2.1c, d}$$

where p is the pressure, v_r, v_φ and v_z are the components of the velocity vector, and μ is the viscosity (different, in the general case, in regions 1 and 2). We, first, proceed with the case of steady homogeneous temperature.

The solution of (2.1) must satisfy the no-slip condition at the boundary of the core Γ_0, as well as the kinematic and dynamic conditions at the boundaries Γ_1 and Γ_2 presented in the form

$$r_i = r_i(\varphi) = R_i + \zeta_i^* = R_i[1+\zeta_i(\varphi, t)], \quad i = 1,2, \tag{2.2}$$

where R_1 and R_2 are the initial outer radii of the cladding and the unpolished outer matrix, respectively.

The above-mentioned no-slip, kinematic and dynamic conditions take the form

$$\Gamma_0: \quad v_{r1} = 0, \quad v_{\varphi 1} = 0 \quad \text{at} \quad r = R_0; \tag{2.3a, b}$$

$$\Gamma_1: \quad v_{r1} = \frac{\partial \zeta_1^*}{\partial t} + \frac{v_{\varphi 1}}{1+\zeta_1}\frac{\partial \zeta_1}{\partial \varphi}, \quad v_{r1} = v_{r2}, \quad v_{\varphi 1} = v_{\varphi 2}, \quad \sigma_{nn1} = \sigma_{nn2} - q_{\alpha 1}, \quad \sigma_{n\tau 1} = \sigma_{n\tau 2}$$
$$\text{at} \quad r = r_1 = R_1 + \zeta_1^*; \tag{2.3c–g}$$

$$\Gamma_2: \quad v_{r2} = \frac{\partial \zeta_2^*}{\partial t} + \frac{v_{\varphi 2}}{1+\zeta_2}\frac{\partial \zeta_2}{\partial \varphi}, \quad \sigma_{nn2} = -q_{\alpha 2}, \quad \sigma_{n\tau 2} = 0 \quad \text{at} \quad r = r_2 = R_2 + \zeta_2^*. \tag{2.3h–j}$$

Here and hereinafter the subscripts 1 and 2 denote quantities relating to the cladding and outer matrix, respectively. The capillary pressures $q_{\alpha 1}$ and $q_{\alpha 2}$ at the boundaries Γ_1 and Γ_2, in accordance with the Laplace equation, are equal to the products of the interfacial (or surface) tension and the sum of principal curvatures of the corresponding boundary surface. The stresses in the liquid material are denoted by σ_{nn} and $\sigma_{n\tau}$, the subscript n referring to the normal to the boundary and τ to the tangent.

Introducing the stream function ψ ($v_r = r^{-1}\partial\psi/\partial\varphi, v_\varphi = -\partial\psi/\partial r$), we reduce (2.1 a, b) to the biharmonic equation for ψ

$$\Delta^2\psi = \frac{\partial^4\psi}{\partial r^4} + \frac{2}{r}\frac{\partial^3\psi}{\partial r^3} - \frac{1}{r^2}\frac{\partial^2\psi}{\partial r^2} + \frac{1}{r^3}\frac{\partial\psi}{\partial r} + \frac{4}{r^4}\frac{\partial^2\psi}{\partial\varphi^2} - \frac{2}{r^3}\frac{\partial^3\psi}{\partial r\,\partial\varphi^2} + \frac{2}{r^2}\frac{\partial^4\psi}{\partial r^2\,\partial\varphi^2} + \frac{1}{r^4}\frac{\partial^4\psi}{\partial\varphi^4} = 0, \tag{2.4}$$

where Δ is the two-dimensional Laplace operator.

The general solution is sought in the form of a Fourier series

$$\psi = \sum_{n=1}^{\infty} f_n(r)(A_n^*\sin n\varphi + B_n^*\cos n\varphi) + f_0(r)(1+S\varphi) + M\varphi$$
$$+ r\varphi(Q_1\sin\varphi + Q_2\cos\phi) + \text{const}, \tag{2.5}$$

where A_n^*, B_n^*, S, M, Q_1 and Q_2 are functions of time.

Substituting (2.5) in (2.4), we arrive at the equation

$$r^4 f_n^{\text{iv}} + 2r^3 f_n''' - r^2 f_n''(1+2n^2) + r f_n'(2n^2+1) + f_n(n^4 - 4n^2) = 0, \tag{2.6}$$

where the primes denote the derivatives with respect to r.

Equation (2.6) is the Euler equation with a general solution in the form

$$f_0(r) = N_1 + N_2\ln r + N_3 r^2 + N_4 r^2\ln r, \tag{2.7a}$$
$$f_1(r) = C_{11}^* r^3 + C_{21}^* r + C_{31}^* r^{-1} + C_{41}^* r\ln r, \tag{2.7b}$$
$$f_n(r) = C_{1n}^* r^{n+2} + C_{2n}^* r^n + C_{3n}^* r^{-n} + C_{4n}^* r^{-n+2}, \quad n \geqslant 2, \tag{2.7c}$$

where C_{1n}^*–C_{4n}^* and N_1–N_4 are arbitrary constants.

By (2.5) and (2.7) we arrive, after some obvious renotation, at the following expressions for the stream functions in the domains 1 and 2:

$$\begin{aligned}\psi_1 = & \sum_{n=2}^{\infty} (r^{n+2}+C_{2n1}r^n+C_{3n1}r^{-n}+C_{4n1}r^{-n+2})[A_n(t)\sin n\varphi - B_n(t)\cos n\varphi] \\ & +(r^3+C_{211}r+C_{311}r^{-1}+C_{411}r\ln r)[A_1(t)\sin\varphi - B_1(t)\cos\varphi] \\ & +N_{11}+N_{21}\ln r+N_{31}r^2+N_{41}r^2\ln r \\ & +M_1\varphi+(L_{11}\ln r+L_{21}r^2+L_{31}r^2\ln r)\varphi+Q_{11}r\varphi\sin\varphi+Q_{12}r\varphi\cos\varphi, \end{aligned} \tag{2.8a}$$

$$\begin{aligned}\psi_2 = & \sum_{n=2}^{\infty} (r^{n+2}+C_{2n2}r^n+C_{3n2}r^{-n}+C_{4n2}r^{-n+2})[D_n(t)\sin n\varphi - E_n(t)\cos n\varphi] \\ & +(r^3+C_{212}r+C_{312}r^{-1}+C_{412}r\ln r)[D_1(t)\sin\varphi - E_1(t)\cos\varphi] \\ & +N_{12}+N_{22}\ln r+N_{32}r^2+N_{42}r^2\ln r \\ & +M_2\varphi+(L_{12}\ln r+L_{22}r^2+L_{32}r^2\ln r)\varphi+Q_{21}r\varphi\sin\varphi+Q_{22}r\varphi\cos\varphi. \end{aligned} \tag{2.8b}$$

Here we have emphasized the dependence of the coefficients of the Fourier series A_n, B_n, D_n and E_n on the time parameter t in the boundary conditions (2.3).

Since the stream function is defined up to an arbitrary constant, we can take in (2.8) $N_{11}=N_{12}=0$.

By using (2.8) we arrive at the following expressions for the velocity components:

$$\begin{aligned}v_{r1} = & \sum_{n=2}^{\infty} (r^{n+1}+C_{2n1}r^{n-1}+C_{3n1}r^{-n-1}+C_{4n1}r^{-n+1})n(A_n\cos n\varphi+B_n\sin n\varphi) \\ & +(r^2+C_{211}+C_{311}r^{-2}+C_{411}\ln r)(A_1\cos\varphi+B_1\sin\varphi) \\ & +\frac{M_1}{r}+\frac{L_{11}}{r}\ln r+L_{21}r+L_{31}r\ln r+Q_{11}(\sin\varphi+\varphi\cos\varphi)+Q_{21}(\cos\varphi-\varphi\sin\varphi), \end{aligned} \tag{2.9a}$$

$$\begin{aligned}v_{\varphi 1} = & -\sum_{n=2}^{\infty} [(n+2)r^{n+1}+nC_{2n1}r^{n-1}-nC_{3n1}r^{-n-1}+(-n+2)C_{4n1}r^{-n+1}] \\ & \times(A_n\sin n\varphi-B_n\cos n\varphi)-(3r^2+C_{211}-C_{311}r^{-2}+C_{411}\ln r+C_{411}) \\ & \times(A_1\sin\varphi-B_1\cos\varphi)-\left(\frac{N_{21}}{r}+2N_{31}r+2N_{41}r\ln r+N_{41}r\right) \\ & -\left(\frac{L_{11}}{r}+2L_{21}r+2L_{31}r\ln r+L_{31}r\right)\varphi-Q_{11}\varphi\sin\varphi-Q_{21}\varphi\cos\varphi, \end{aligned} \tag{2.9b}$$

$$\begin{aligned}v_{r2} = & \sum_{n=2}^{\infty} (r^{n+1}+C_{2n2}r^{n-1}+C_{3n2}r^{-n-1}+C_{4n2}r^{-n+1})n(D_n\cos n\varphi+E_n\sin n\varphi) \\ & +(r^2+C_{212}+C_{312}r^{-2}+C_{412}\ln r)(D_1\cos\varphi+E_1\sin\varphi) \\ & +\frac{M_2}{r}+\frac{L_{12}}{r}\ln r+L_{22}r+L_{32}r\ln r+Q_{12}(\sin\varphi+\varphi\cos\varphi)+Q_{22}(\cos\varphi-\varphi\sin\varphi), \end{aligned} \tag{2.9c}$$

$$v_{\varphi 2} = -\sum_{n=2}^{\infty} [(n+2)\, r^{n+1} + nC_{2n2}\, r^{n-1} - nC_{3n2}\, r^{-n-1} + (-n+2)\, C_{4n2}\, r^{-n+1}]$$

$$\times (D_n \sin n\varphi - E_n \cos n\varphi) - (3r^2 + C_{212} - C_{312}\, r^{-2} + C_{412} \ln r + C_{412})$$

$$\times (D_1 \sin\varphi - E_1 \cos\varphi) - \left(\frac{N_{22}}{r} + 2N_{32}\, r + 2N_{42}\, r \ln r + N_{42}\, r\right)$$

$$-\left(\frac{L_{12}}{r} + 2L_{22}\, r + 2L_{32}\, r \ln r + L_{32}\, r\right)\varphi - Q_{21}\,\varphi \sin\varphi - Q_{22}\,\varphi \cos\varphi. \qquad (2.9d)$$

Here and hereinafter, dependence of A_n, B_n, D_n and E_n on t is understood.

In order to satisfy the condition of periodicity of the velocity field with respect to φ, the coefficients $Q_{1i} = Q_{2i} = L_{1i} = L_{2i} = L_{3i} = 0$ $(i = 1, 2)$, as can be seen from (2.9b) and (2.9d). All axisymmetric terms with the coefficients N_{ij} in (2.9b) and (2.9d) correspond to rotations of a whole material layer (a ring) in the preform (including, in particular, a quasi-rigid rotation of the preform as a whole). Such an axisymmetric motion cannot arise under the action of non-axisymmetric polishing, and thus $N_{2i} = N_{4i} = 0$ $(i = 1, 2)$. (The latter evidently follows if one proceeds with the problem including N_{2i} and N_{4i} and then satisfies the boundary conditions at the interfaces.) An imposed rigid-body rotation of the preform as a whole in the inertialess situation cannot affect the shape of the boundaries. Therefore, without loss of generality, we can assume that $N_{3i} = 0$ $(i = 1, 2)$.

The sink-like term M_1/r in (2.9a) should disappear since the rigid core does not allow such a component to exist in the domain of cladding (in the two-layer preform this term should also disappear since velocity v_{r1} should be finite at $r = 0$). Thus, $M_1 = 0$ and, via the interfacial conditions, $M_2 = 0$ in (2.9c).

Substituting (2.9) in (2.1a, b), we find the pressure

$$p_1 = \mu_1 \left\{ \sum_{n=2}^{\infty} [r^n (4n+4) + C_{4n1}\, r^{-n} (4n-4)] (A_n \cos n\varphi + B_n \sin n\varphi) \right.$$
$$\left. + \left(8r - \frac{2C_{411}}{r}\right)(A_1 \cos\varphi + B_1 \sin\varphi)\right\} + K_1, \qquad (2.10a)$$

$$p_2 = \mu_2 \left\{ \sum_{n=2}^{\infty} [r^n (4n+4) + C_{4n2}\, r^{-n} (4n-4)] (D_n \cos n\varphi + E_n \sin n\varphi) \right.$$
$$\left. + \left(8r - \frac{2C_{412}}{r}\right)(D_1 \cos\varphi + E_1 \sin\varphi)\right\} + K_2, \qquad (2.10b)$$

where μ_1 and μ_2 are the viscosities in the domains of the cladding and the outer matrix, respectively; K_1 and K_2 are constants.

By means of (2.9) and (2.10) we arrive at the following expressions for the stresses:

$$\sigma_{rr} = -p + 2\mu\, \partial v_r/\partial r, \quad \sigma_{r\varphi} = \mu (r^{-1}\, \partial v_r/\partial\varphi + \partial v_\varphi/\partial r - v_\varphi/r):$$

$$\sigma_{rr1} = \mu_1 \sum_{n=2}^{\infty} [r^n (-2n - 4 + 2n^2) + C_{2n1}\, r^{n-2} (2n^2 - 2n)$$
$$+ C_{3n1}\, r^{-n-2} (-2n^2 - 2n) + C_{4n1}\, r^{-n} (-2n + 4 - 2n^2)] (A_n \cos n\varphi + B_n \sin n\varphi)$$
$$+ \mu_1 (-4r + 4C_{411}/r - 4C_{311}\, r^{-3})(A_1 \cos\varphi + B_1 \sin\varphi) - K_1, \qquad (2.11a)$$

$$\sigma_{r\varphi 1} = \mu_1 \left\{ \sum_{n=2}^{\infty} [r^n(-2n^2-2n) + C_{2n1} r^{n-2}(-2n^2+2n) + C_{3n1} r^{-n-2}(-2n^2-2n) + C_{4n1} r^{-n}(-2n^2+2n)] \times (A_n \sin n\varphi - B_n \cos n\varphi) - (4r + 4C_{311} r^{-3})(A_1 \sin\varphi - B_1 \cos\varphi) \right\}. \tag{2.11b}$$

The expressions for σ_{rr2} and $\sigma_{r\varphi 2}$ are analogous to (2.11 a) and (2.11 b) with σ_{rr2}, $\sigma_{r\varphi 2}$, μ_2, D_n and E_n instead of σ_{rr1}, $\sigma_{r\varphi 1}$, μ_1, A_n and B_n, respectively.

We linearize the problem, assuming $\zeta_i \ll 1$ and neglecting small terms of higher order. Then the boundary conditions (2.3) and the expressions for capillary pressure reduce to the form

$$\Gamma_0: \quad v_{r1} = 0, \quad v_{\varphi 1} = 0 \quad \text{at} \quad r = R_0; \tag{2.12a, b}$$

$$\Gamma_1: \quad v_{r1} = \frac{\partial \zeta_1^*}{\partial t}, \quad v_{r1} = v_{r2}, \quad v_{\varphi 1} = v_{\varphi 2}, \quad \sigma_{rr1} = \sigma_{rr2} - q_{\alpha 1}, \quad \sigma_{r\varphi 1} = \sigma_{r\varphi 2} \quad \text{at} \quad r = R_1; \tag{2.12c–g}$$

$$\Gamma_2: \quad v_{r2} = \frac{\partial \zeta_2^*}{\partial t}, \quad \sigma_{rr2} = -q_{\alpha 2}, \quad \sigma_{r\varphi 2} = 0 \quad \text{at} \quad r = R_2; \tag{2.12h–j}$$

$$q_{\alpha i} = \frac{\alpha_i}{R_i}(1-\zeta_i) - \frac{\alpha_i}{R_i}\frac{\partial^2 \zeta_i}{\partial \varphi^2}, \quad i = 1, 2, \tag{2.12k}$$

where α_1 and α_2 are the interfacial tension at the boundary Γ_1 and the surface tension at the boundary Γ_2, respectively.

We represent the perturbations of the boundaries in the form of Fourier series

$$\zeta_1 = \frac{b_{01}(t)}{2} + \sum_{n=1}^{\infty} [a_{n1}(t) \sin n\varphi + b_{n1}(t) \cos n\varphi], \tag{2.13a}$$

$$\zeta_2 = \frac{b_{02}(t)}{2} + \sum_{n=1}^{\infty} [a_{n2}(t) \sin n\varphi + b_{n2}(t) \cos n\varphi], \tag{2.13b}$$

and thus, via (2.9), (2.11)–(2.13) we obtain for $n = 0$†

$$b_{01} = b_{010}, \quad b_{02} = b_{020} \tag{2.14a, b}$$

(here and hereinafter the additional subscript 0 stands for $t = 0$); for $n = 1$

$$b_{11} = b_{110}, \quad b_{12} = b_{120}, \tag{2.15a, b}$$

whereas for $n \geqslant 2$ we arrive at the system of two differential equations for determining the coefficients b_{n1} and b_{n2}:

$$k_1 \frac{\mathrm{d}b_{n1}}{\mathrm{d}t} + k_2 \frac{\mathrm{d}b_{n2}}{\mathrm{d}t} + k_3 b_{n2} + k_4 b_{n1} = 0, \tag{2.16a}$$

$$k_5 \frac{\mathrm{d}b_{n1}}{\mathrm{d}t} + k_6 \frac{\mathrm{d}b_{n2}}{\mathrm{d}t} + k_7 b_{n2} + k_8 b_{n1} = 0. \tag{2.16b}$$

Here we adopt the notation given in Appendix A.

† The related derivations can be obtained on request from the author or from the Journal of Fluid Mechanics editorial office.

Solving the system (2.16) and introducing the notation

$$l_{11} = \frac{k_2 k_7 - k_3 k_6}{k_1 k_6 - k_2 k_5}, \quad l_{12} = \frac{k_2 k_8 - k_4 k_6}{k_1 k_6 - k_2 k_5}, \quad l_{21} = \frac{k_3 k_5 - k_1 k_7}{k_1 k_6 - k_2 k_5}, \quad l_{22} = \frac{k_4 k_5 - k_1 k_8}{k_1 k_6 - k_2 k_5} \qquad (2.17\,a\text{–}d)$$

for $n \geqslant 2$, when $\alpha_1 \neq 0$ (and hence $l_{22} \neq 0$), we obtain

$$b_{n1} = \frac{P^+(m^+ - l_{21})}{l_{22}} \exp(m^+ t) + \frac{P^-(m^- - l_{21})}{l_{22}} \exp(m^- t), \qquad (2.18\,a)$$

$$b_{n2} = P^+ \exp(m^+ t) + P^- \exp(m^- t), \qquad (2.18\,b)$$

$$m^\pm = \frac{l_{21} + l_{12}}{2} \pm \left[\frac{(l_{21} + l_{12})^2}{4} + l_{22} l_{11} - l_{21} l_{12}\right]^{1/2}. \qquad (2.18\,c)$$

The constants P^+ and P^- are determined by the initial perturbations of the boundaries ζ_1 and ζ_2 (at $t = 0$). Their Fourier coefficients, denoted as in (2.14) and (2.15) by the additional subscript 0, are known. Thus, we arrive at

$$P^+ = \frac{b_{n20}(m^- - l_{21}) - b_{n10} l_{22}}{m^- - m^+}, \quad P^- = \frac{b_{n10} l_{22} - b_{n20}(m^+ - l_{21})}{m^- - m^+}. \qquad (2.19\,a, b)$$

In the particular case, $\alpha_1 = 0$ ($l_{22} = 0$) the coefficients b_{n2} are calculated as before, using (2.18*b*) and (2.19), whereas b_{n1} is found from the expression

$$b_{n1} = b_{n10} + b_{n20} \frac{l_{11}}{l_{21}} [\exp(l_{21} t) - 1], \quad n \geqslant 2. \qquad (2.20)$$

The expressions for coefficients a_{n1} and a_{n2} will be (2.14), (2.15), and (2.18)–(2.20) with b_{n1} and b_{n2} replaced with a_{n1} and a_{n2}, respectively.

In the case $\gamma_0 = R_0/R_1 = 0$ the solution obtained for a three-layer preform reduces to that of a two-layer one. In the latter there are only the cladding and outer matrix, whereas the core is negligibly small.

Naturally, in the case $\gamma_0 = 0$, $\mu_1 = \mu_2$ and $\alpha_1 = 0$ the solutions for a three- and a two-layer preform reduce to that of a single-layer preform

$$b_{02} = b_{020}, \quad a_{12} = a_{120}, \quad b_{12} = b_{120}, \qquad (2.21\,a\text{–}c)$$

$$n \geqslant 2, \quad a_{n2} = a_{n20} \exp\left(-\frac{\alpha_2 n}{2\mu_2 R_2} t\right), \quad b_{n2} = b_{n20} \exp\left(-\frac{\alpha_2 n}{2\mu_2 R_2} t\right). \qquad (2.21\,d, e)$$

This solution is of interest in such applications as formation of non-circular textile fibres (Ziabicki 1976).

In addition, we generalize the solution (2.18)–(2.20) obtained above to the case of a two-layer preform drawn uniaxially and uniformly into a fibre with simultaneous structural changes in the cross-section taking place. We assume that along the fibre axis z there exists a velocity v_z such that $\partial v_z/\partial z = D_{zz}(t)$, $\partial v_z/\partial r = \partial v_z/\partial \varphi = 0$ and $\partial v_r/\partial z = \partial v_\varphi/\partial z = 0$. Formally we consider the case of a slow uniform stretching, for example by two clamps moving in opposite directions when v_r, v_φ and an area of the preform cross-section are independent of z, whereas v_z is constant over the cross-section. In fibre drawing by a receiving bobbin from a heated preform, all the above assumptions are applicable only when variation of the parameters along a spinline is gradual, which is the case under certain conditions (Yarin 1993).

The projections of the momentum equations (2.1*a*) and (2.1*b*) accordingly remain unchanged. The projection of the momentum equation on the z-axis in the given case takes the form $\partial p/\partial z = 0$, whereas the continuity equation is the following:

$$\frac{\partial r v_r}{\partial r} + \frac{\partial v_\varphi}{\partial \varphi} + r D_{zz} = 0. \tag{2.22}$$

Clearly, all equations and boundary conditions are satisfied if to the velocities v_{r1} and v_{r2} used above we add terms $(-rD_{zz}/2)$, leaving $v_{\varphi 1}$ and $v_{\varphi 2}$ unchanged. In the given case

$$R_1 = R_{10} \exp\left[-\frac{1}{2}\int_0^t D_{zz}(t'')\,\mathrm{d}t''\right], \quad R_2 = R_{20} \exp\left[-\frac{1}{2}\int_0^t D_{zz}(t'')\,\mathrm{d}t''\right]. \tag{2.23a, b}$$

The basic set of differential equations to which the problem reduces retains the form (2.16), as time differentiation is present only for conditions (2.12c, h), which lead to the two first terms with the time derivatives on the left in (2.16a, b); the coefficients k_i in (2.16) can in principle be time dependent. It is only necessary to account for the fact that now, via (2.23), $\gamma = R_2/R_1 = R_{20}/R_{10}$, which means that γ is time independent in spite of the fact that R_1 and R_2 are functions of time. The ratios α_1/α_2 and μ_1/μ_2 are constant, whereas $\gamma_0 = 0$. From (A 1) of Appendix A we see that among all the coefficients S_1–S_{17}, only S_5, S_6, S_{11} and S_{14} are time dependent, since they are proportional to the factor $\alpha_2/(\mu_2 R_2)$. Therefore, via (A 2) we see that among all the coefficients k_1–k_8 only k_3, k_4, k_7 and k_8 are time dependent and all of them are proportional to the factor

$$\alpha_2/(\mu_2 R_2) = [\alpha_2/(\mu_2 R_{20})] \exp\left[\frac{1}{2}\int_0^t D_{zz}(t'')\,\mathrm{d}t''\right].$$

Thus if we replace t in (2.16) by a new time

$$t_1 = \int_0^t \exp\left[\frac{1}{2}\int_0^{t'} D_{zz}(t'')\,\mathrm{d}t''\right]\mathrm{d}t', \tag{2.24}$$

then equations (2.16) retain their previous form (with t_1 instead of t), whereas the coefficients k_3, k_4, k_7 and k_8 take a new time-independent form given by (A 1h, i, n, q) with R_{20} instead of R_2, and (A 2c, d, g, h).

In the case in question the coefficients of the Fourier series depend exponentially not on t but on t_1. Thus, the solution of the problem is now given by (2.14), (2.15), (2.17)–(2.20), (A 1) and (A 2) with t replaced with t_1, with $\gamma = R_{20}/R_{10}$ and with R_{20} instead of R_2 in (A 1h, i, n, q). Consequently, the dimensions of non-symmetrical cladding in an undrawn preform, divided say by $R \equiv R_{20}$, are the same as those of the cladding in the fibre drawn from it, divided by R_2. Only the time taken to reach such a shape will vary.

The same conclusion applies to the case of viscosity variation with time. Indeed, at the beginning of the present section it was shown that the preform is practically uniformly heated over the cross-section (this is also applicable to the case of a spinline or a fibre drawn from it). In the case of an overheat and equal activation energies, $U_1 = U_2$, this leads to a time-independent ratio $\mu_1/\mu_2 = \mu_{10}/\mu_{20}$, whereas variation of α_1/α_2 is negligible and $\gamma_0 = 0$. Under these conditions the coefficients k_3, k_4, k_7 and k_8 are proportional to $\alpha_2/(\mu_2 R_2) = [\alpha_2/(\mu_{20} R_2)] \exp[-U_2/R_g T(t)]$. Then, replacing t in (2.16) by a new time

$$t_2 = \int_0^t \exp[-U_2/R_g T(t'')]\,\mathrm{d}t'' \tag{2.25}$$

we preserve the form of equations (2.16) (with t_2 instead of t), whereas the coefficients k_3, k_4, k_7 and k_8 take a new time-independent form given by (A 1*h*, *i*, *n*, *q*) with μ_{20} instead of μ_2, and (A 2*c*, *d*, *g*, *h*).

3. Surface-tension-driven collapse of non-symmetric composite tubes

In this section we analyse the surface-tension-driven collapse of a tube with a coating inside (see figure 2). All the estimates given at the beginning of the previous section hold in the present case, and thus the process is considered as planar and quasi-steady creeping flow. It is supposed that there is a vacuum both inside and outside the tube, or that there is a gas which can leak out from the tube through the open ends and its dynamic effect is negligible.

The problem concerns the fact that the inner surface of the deposited coating may differ from a circle, as a result of which the other two interfaces may be rather severely changed. In turn, as a result, the collapsed coating may for some time not be a circle.

The flow is described by the biharmonic equation (2.4) for the stream function in each domain, 1 or 2. Its general solution is given by (2.8) where the additional subscripts 1 and 2 refer to the domain of the coating and tube material, respectively.

By the same reasoning as in §2 $Q_{1i} = Q_{2i} = L_{1i} = L_{2i} = L_{3i} = N_{1i} = N_{2i} = N_{3i} = N_{4i} = 0, (i = 1,2)$ and from (2.8) we get

$$\psi_1 = \sum_{n=2}^{\infty} (r^{n+2} + C_{2n1} r^n + C_{3n1} r^{-n} + C_{4n1} r^{-n+2})(A_n \sin n\varphi - B_n \cos n\varphi)$$
$$+ (r^3 + C_{211} r + C_{311} r^{-1} + C_{411} r \ln r)(A_1 \sin\varphi - B_1 \cos\varphi) + M_1 \varphi, \quad (3.1a)$$

$$\psi_2 = \sum_{n=2}^{\infty} (r^{n+2} + C_{2n2} r^n + C_{3n2} r^{-n} + C_{4n2} r^{-n+2})(D_n \sin n\varphi - E_n \cos n\varphi)$$
$$+ (r^3 + C_{212} r + C_{312} r^{-1} + C_{412} r \ln r)(D_1 \sin\varphi - E_1 \cos\varphi) + M_2 \varphi. \quad (3.1b)$$

The following velocity components correspond to the solution (3.1):

$$v_{r1} = \sum_{n=2}^{\infty} (r^{n+1} + C_{2n1} r^{n-1} + C_{3n1} r^{-n-1} + C_{4n1} r^{-n+1})\, n(A_n \cos n\varphi + B_n \sin n\varphi)$$
$$+ (r^2 + C_{211} + C_{311} r^{-2} + C_{411} \ln r)(A_1 \cos\varphi + B_1 \sin\varphi) + M_1/r, \quad (3.2a)$$

$$v_{\varphi 1} = -\sum_{n=2}^{\infty} [(n+2)\, r^{n+1} + nC_{2n1} r^{n-1} - nC_{3n1} r^{-n-1} + (-n+2)\, C_{4n1} r^{-n+1}]$$
$$\times (A_n \sin n\varphi - B_n \cos n\varphi) - [3r^2 + C_{211} - C_{311} r^{-2} + C_{411}(\ln r + 1)](A_1 \sin\varphi - B_1 \cos\varphi), \quad (3.2b)$$

$$v_{r2} = \sum_{n=2}^{\infty} (r^{n+1} + C_{2n2} r^{n-1} + C_{3n2} r^{-n-1} + C_{4n2} r^{-n+1})\, n(D_n \cos n\varphi + E_n \sin n\varphi)$$
$$+ (r^2 + C_{212} + C_{312} r^{-2} + C_{412} \ln r)(D_1 \cos\varphi + E_1 \sin\varphi) + M_2/r, \quad (3.2c)$$

$$v_{\varphi 2} = -\sum_{n=2}^{\infty} [(n+2)\, r^{n+1} + nC_{2n2} r^{n-1} - nC_{3n2} r^{-n-1} + (-n+2)\, C_{4n2} r^{-n+1}]$$
$$\times (D_n \sin n\varphi - E_n \cos n\varphi) - [3r^2 + C_{212} - C_{312} r^{-2} + C_{412}(\ln r + 1)](D_1 \sin\varphi - E_1 \cos\varphi). \quad (3.2d)$$

Note that in the given case there are no restrictions on the sink-like components $M_i/r\,(i=1,2)$ in (3.2*a*) and (3.2*c*), since we consider a hollow preform. Thus these terms survive here in contrast to the case considered in §2.

Calculating the pressure from the Stokes equations by using (2.1*a*, *b*) and (3.2) and then the stress components σ_{rr} and $\sigma_{r\varphi}$ in each of the domains, we arrive at

$$\begin{aligned}\sigma_{rr1} = \mu_1 \sum_{n=2}^{\infty} [&r^n(-2n-4+2n^2)+C_{2n1}r^{n-2}(2n^2-2n)+C_{3n1}r^{-n-2}(-2n^2-2n)\\ &+C_{4n1}r^{-n}(-2n+4-2n^2)](A_n\cos n\varphi+B_n\sin n\varphi)\\ &+\mu_1(-4r+4C_{411}r^{-1}-4C_{311}r^{-3})(A_1\cos\varphi+B_1\sin\varphi)-K_{10}-2\mu_1 M_1 r^{-2},\end{aligned} \tag{3.3a}$$

$$\begin{aligned}\sigma_{rr2} = \mu_2 \sum_{n=2}^{\infty} [&r^n(-2n-4+2n^2)+C_{2n2}r^{n-2}(2n^2-2n)+C_{3n2}r^{-n-2}(-2n^2-2n)\\ &+C_{4n2}r^{-n}(-2n+4-2n^2)](D_n\cos n\varphi+E_n\sin n\varphi)\\ &+\mu_2(-4r+4C_{412}r^{-1}-4C_{312}r^{-3})(D_1\cos\varphi+E_1\sin\varphi)-K_{20}-2\mu_2 M_2 r^{-2},\end{aligned} \tag{3.3b}$$

$$\begin{aligned}\sigma_{r\varphi1} = \mu_1 \sum_{n=2}^{\infty} [&-2r^n(n^2+n)+2C_{2n1}r^{n-2}(-n^2+n)+2C_{3n1}r^{-n-2}(-n^2-n)\\ &+2C_{4n1}r^{-n}(n-n^2)](A_n\sin n\varphi-B_n\cos n\varphi)\\ &+\mu_1(-4r-4C_{311}r^{-3})(A_1\sin\varphi-B_1\cos\varphi),\end{aligned} \tag{3.3c}$$

$$\begin{aligned}\sigma_{r\varphi2} = \mu_2 \sum_{n=2}^{\infty} [&-2r^n(n^2+n)+2C_{2n2}r^{n-2}(-n^2+n)+2C_{3n2}r^{-n-2}(-n^2-n)\\ &+2C_{4n2}r^{-n}(n-n^2)](D_n\sin n\varphi-E_n\cos n\varphi)\\ &+\mu_2(-4r-4C_{312}r^{-3})(D_1\sin\varphi-E_1\cos\varphi).\end{aligned} \tag{3.3d}$$

Here K_{10} and K_{20} are constants, and μ_1 and μ_2 are the viscosities of the liquid glass in the domains of the coating and tube material, respectively.

The perturbations of the radii of the interfaces Γ_0, Γ_1 and Γ_2 (see figure 2) are given by the expression

$$r_i = R_i(t)[1+\zeta_i(\varphi,t)], \quad i=0,1,2, \tag{3.4}$$

where r_i is the modulus of the radius vector of the perturbed interface, $R_i(t)$ the radius vector of the unperturbed interface (the circle), and t time (cf. (2.2)).

The kinematic boundary condition at all interfaces has the form

$$v_r|_{r_i=R_i(1+\zeta_i)} = \frac{\mathrm{d}R_i}{\mathrm{d}t}+\frac{\mathrm{d}R_i}{\mathrm{d}t}\zeta_i+R_i\frac{\partial \zeta_i}{\partial t} \tag{3.5}$$

(cf. (2.12*c*, *h*)).

Here and hereinafter, the boundary perturbations are assumed small, and the boundary conditions are linearized.

Further, we have the conditions

$$v_{r1}=v_{r2}, \quad v_{\varphi1}=v_{\varphi2} \quad \text{at} \quad r=r_1=R_1(1+\zeta_1) \tag{3.6a, b}$$

(cf. (2.12*d*, *e*)).

The dynamical boundary conditions are as follows:

$$\sigma_{rr1}=q_{\alpha0}, \quad \sigma_{r\varphi1}=0 \quad \text{at} \quad r=r_0=R_0(1+\zeta_0), \tag{3.7a, b}$$

$$\sigma_{rr1}=\sigma_{rr2}-q_{\alpha1}, \quad \sigma_{r\varphi1}=\sigma_{r\varphi2} \quad \text{at} \quad r=r_1=R_1(1+\zeta_1), \tag{3.7c, d}$$

$$\sigma_{rr2}=-q_{\alpha2}, \quad \sigma_{r\varphi2}=0 \quad \text{at} \quad r=r_2=R_2(1+\zeta_2), \tag{3.7e, f}$$

where $q_{\alpha i}$ are the capillary pressures defined by the linearized Laplace formula (cf. (2.12*f, g, i, j*)).

Consider, first, the unperturbed part of (3.2)–(3.7). After calculation of the constants M_1, M_2, K_{10} and K_{20}, we obtain the equations describing the evolution of the radii of the unperturbed interfaces (circles) during the collapse of a tube with a coating inside:

$$\frac{\mathrm{d}\bar{R}_0}{\mathrm{d}\bar{t}} = \frac{\gamma_1^2}{\bar{R}_0}F, \quad \frac{\mathrm{d}\bar{R}_1}{\mathrm{d}\bar{t}} = \frac{\gamma_*^2}{\bar{R}_1}F, \quad \frac{\mathrm{d}\bar{R}_2}{\mathrm{d}\bar{t}} = \frac{1}{\bar{R}_2}F, \tag{3.8a–c}$$

$$F = \frac{1}{2}\frac{\bar{R}_2^{-1}+\gamma_*\bar{\alpha}_1\bar{R}_1^{-1}+\gamma_1\bar{\alpha}_0\bar{R}_0^{-1}}{\bar{\mu}_1(\gamma_*^2\bar{R}_1^{-2}-\gamma_1^2\bar{R}_0^{-2})+(\bar{R}_2^{-2}-\gamma_*^2\bar{R}_1^{-2})} \tag{3.8d}$$

(F is always negative).

Here the following non-dimensional variables are introduced:

$$\bar{\alpha}_0 = \alpha_0/\alpha_2, \quad \bar{\alpha}_1 = \alpha_1/\alpha_2, \quad \bar{\mu}_1 = \mu_1/\mu_2, \tag{3.9a–c}$$

$$\gamma_* = R_{20}/R_{10}, \quad \gamma_1 = R_{20}/R_{00}, \tag{3.9d, e}$$

$$\bar{R}_0 = R_0/R_{00}, \quad \bar{R}_1 = R_1/R_{10}, \quad \bar{R}_2 = R_2/R_{20}, \quad \bar{t} = t\alpha_2/\mu_2 R_{20}. \tag{3.9f–i}$$

The surface-tension coefficients at the interfaces Γ_i are denoted α_i, and the initial values (at $t = 0$) of the radii of the unperturbed interfaces (circles) R_i are denoted R_{i0}.

In the particular case $\bar{\alpha}_0 = 1$, $\bar{\alpha}_1 = 0$, $\bar{\mu}_1 = 1$ (the single-phase tube), (3.8) have an analytical solution, as follows:

$$\bar{R}_0 = \tfrac{1}{2}\gamma_1\left[\frac{1-\gamma_1^{-2}}{1-\gamma_1^{-1}+\frac{1}{2}\bar{t}}-(1-\gamma_1^{-1}+\tfrac{1}{2}\bar{t})\right], \quad \bar{R}_2 = \frac{1}{2}\left[\frac{1-\gamma_1^{-2}}{1-\gamma_1^{-1}+\frac{1}{2}\bar{t}}+(1-\gamma_1^{-1}+\tfrac{1}{2}\bar{t})\right], \tag{3.10a, b}$$

which shows that the tube will collapse completely after a time

$$\bar{t}_* = -2(1-\gamma_1^{-1})+2(1-\gamma_1^{-2})^{1/2}. \tag{3.11}$$

In another particular case when $\bar{\alpha}_0 = 1$, $\bar{\alpha}_1 = 0$, and $\bar{\mu}_1$ is arbitrary, equation (3.8*a*) is identical with (6) of Lewis (1977) with the pressure differential equal to zero.

For all three interfaces, we consider perturbations in the form of the Fourier series (cf. (2.13)):

$$\zeta_i = \frac{b_{0i}(t)}{2}+\sum_{n=1}^{\infty}[a_{ni}(t)\sin n\varphi+b_{ni}(t)\cos n\varphi], \quad i = 0,1,2. \tag{3.12}$$

By using (3.2), (3.3) and (3.12) we satisfy the boundary conditions (3.5)–(3.7) and arrive at the following results.† For the $n = 0$ mode of the interfaces we obtain the following differential equations:

$$\frac{\mathrm{d}b_{00}}{\mathrm{d}\bar{t}} = -\frac{2}{\bar{R}_0}\frac{\mathrm{d}\bar{R}_0}{\mathrm{d}\bar{t}}b_{00}+\frac{\gamma_1^2}{\bar{R}_0^2}F_1, \quad \frac{\mathrm{d}b_{01}}{\mathrm{d}\bar{t}} = -\frac{2}{\bar{R}_1}\frac{\mathrm{d}\bar{R}_1}{\mathrm{d}\bar{t}}b_{01}+\frac{\gamma_*^2}{\bar{R}_1^2}F_1, \quad \frac{\mathrm{d}b_{02}}{\mathrm{d}\bar{t}} = -\frac{2}{\bar{R}_2}\frac{\mathrm{d}\bar{R}_2}{\mathrm{d}\bar{t}}b_{02}+\frac{1}{\bar{R}_2^2}F_1, \tag{3.13a–c}$$

$$F_1 = -\frac{1}{2}\frac{1}{\bar{\mu}_1\gamma_*^2\bar{R}_1^{-2}-\bar{\mu}_1\gamma_1^2\bar{R}_0^{-2}-\gamma_*^2\bar{R}_1^{-2}+\bar{R}_2^{-2}}\left[b_{00}\left(\frac{\bar{\alpha}_0\gamma_1}{\bar{R}_0}+\frac{4\bar{\mu}_1}{\bar{R}_0}\frac{\mathrm{d}\bar{R}_0}{\mathrm{d}\bar{t}}\right)\right.$$
$$\left.+b_{01}\left(\frac{\bar{\alpha}_1\gamma_*}{\bar{R}_1}+(1-\bar{\mu}_1)\frac{4}{\bar{R}_1}\frac{\mathrm{d}\bar{R}_1}{\mathrm{d}\bar{t}}\right)+b_{02}\left(\frac{1}{\bar{R}_2}-\frac{4}{\bar{R}_2}\frac{\mathrm{d}\bar{R}_2}{\mathrm{d}\bar{t}}\right)\right]. \tag{3.13d}$$

† The related derivations can be obtained on request from the author or from the Journal of Fluid Mechanics editorial office.

For $n = 1$, the following equations are obtained:

$$\frac{\mathrm{d}b_{11}}{\mathrm{d}\bar{t}} = \frac{(Z_2 Z_7 - Z_3 Z_6) b_{12} + (Z_2 Z_8 - Z_4 Z_6) b_{11}}{Z_1 Z_6 - Z_2 Z_5}, \tag{3.14a}$$

$$\frac{\mathrm{d}b_{12}}{\mathrm{d}\bar{t}} = \frac{(Z_3 Z_5 - Z_1 Z_7) b_{12} + (Z_4 Z_5 - Z_1 Z_8) b_{11}}{Z_1 Z_6 - Z_2 Z_5}, \tag{3.14b}$$

$$b_{10} = \Phi_3 b_{11}, \tag{3.14c}$$

where the notation is as in Appendix B.

For $n \geqslant 2$ we find

$$\frac{\mathrm{d}b_{n0}}{\mathrm{d}\bar{t}} = \frac{1}{F_4}(F_3 k_1 k_6 + F_6 k_2 k_9 + F_1' k_5 k_{10} - F_1' k_6 k_9 - F_2 k_{10} k_1 - F_3 k_5 k_2), \tag{3.15a}$$

$$\frac{\mathrm{d}b_{n1}}{\mathrm{d}\bar{t}} = \frac{1}{F_4}(F_1' k_6 k_{11} + F_3 k_2 k_8' + F_2 k_4' k_{10} - F_3 k_6 k_4' - F_1' k_{10} k_8' - F_2 k_2 k_{11}), \tag{3.15b}$$

$$\frac{\mathrm{d}b_{n2}}{\mathrm{d}\bar{t}} = \frac{1}{F_4}(F_2 k_1 k_{11} + F_1' k_8' k_9 + F_3 k_4' k_5 - F_2 k_9 k_4' - F_3 k_8' k_1 - F_1' k_{11} k_5), \tag{3.15c}$$

where the notation is as in Appendix C.

We emphasize that the equations describing the time evolution of the Fourier coefficients a_{ni} may be obtained from (3.14), (3.15), (C 1) and (C 2) by replacing all the coefficients b_{ni} with a_{ni}.

Hence, to describe the evolution of the interfaces Γ_i during the collapse of a tube with a coating inside, we have to integrate numerically the set of ordinary differential equations (3.8), (3.13), (3.14) and (3.15) (for b_{ni} as well as for a_{ni}). The Runge–Kutta method of fourth and fifth order with automatic step size control was used (Forsythe, Malcolm & Moler 1977).

4. Results, discussion and comparison with experimental data

4.1. *Method of polishing*

In the present section the results obtained above are applied to several particular examples. To calculate particular cases, one has to employ data on the material properties of molten glass, such as viscosity, surface and interfacial tension. Determination of surface and interfacial tension of molten glass involves experimental difficulties owing to the necessary high temperatures and high viscosity. The following facts are known from the literature (e.g. Morey 1938, 1954; Scholze 1991): the surface tension of molten glass is practically temperature independent (an increase of 100 K reduces surface tension by about 1–3 %); its variation due to the effect of added oxides (such as B_2O_3, which is considered below) is typically small, of order of several percent; to the best of our knowledge, there is no direct measurements of interfacial tension between two molten glasses. Accordingly, one can virtually neglect surface-tension gradients in non-isothermal problems, and expect that interfacial tension is small compared with surface tension.

The interfacial tension of molten glasses has been measured indirectly by Grigor'yants *et al.* (1989). The experiments were carried out with two-layer quartz optical fibres with borosilicate quartz glass in the cladding and pure quartz in the outer matrix. Fibres with non-circular cladding formed by the polishing method were

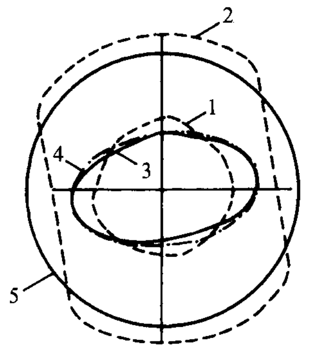

FIGURE 3. Two-layer preform formation – comparison with the experiment. The dashed curves 1 and 2 show the configuration of the boundaries of the cladding and outer matrix at the initial time. The solid curve 3 shows the computed steady-state shape of the boundary of the cladding after rounding-off of softened preform under the action of surface tension. Curve 4 shows the final shape of the boundary of the cladding which was observed in the experiment, and curve 5 shows the circumference of the outer matrix of the preform after rounding-off both in the theory and experiment. Experimental data of Grigor'yants *et al.* (1989): $\alpha_1/\alpha_2 = 0$, $\mu_1/\mu_2 = 0.2$, and $\gamma = 2.27$.

subjected to prolonged heating. No rounding-off of the boundary of the cladding was observed in this experiment, which shows that interfacial tension between borosilicate quartz glass and pure quartz is, indeed, approximately zero. For this reason the case $\alpha_1/\alpha_2 = 0$ is considered below as a basic one. The solutions obtained in §§2 and 3 allow us, however, to treat the cases with $\alpha_1/\alpha_2 \neq 0$. The results of these calculations are also discussed.

First, we consider two-layer preforms. This case corresponds to the solution given by (2.14), (2.15), (2.17)–(2.20), (A 1) and (A 2) with $\gamma_0 = 0$. We compare theoretical results with the experimental data of Grigor'yants *et al.* (1989) corresponding to the case $\alpha_1/\alpha_2 = 0$, $\mu_1/\mu_2 = 0.2$, and $\gamma = 2.27$. The comparison is presented in figure 3 and shows that the calculations agree fairly well with the experimental data. The satisfactory agreement of calculations with experimental data for large initial perturbations of the circular outer boundary of the preform, as shown in figure 3, shows that the analytical solution obtained is sufficiently accurate far beyond a linear approximation. Note also that the value $\alpha_1/\alpha_2 = 0$ used in the calculation is in agreement with the experiment on prolonged heating of the preform discussed above.

The results shown in figures 3–5 were obtained with 19 modes of the Fourier series.

In figure 4 we present some additional characteristic calculation results for two-layer preforms. The corresponding values of the parameters are shown in table 1.

It is emphasized that the analysis in the present work is based on the assumption that each interface is a small perturbation of a circle and most of the cases in figure 4 are, indeed, moderate perturbations of circles. The question of the range of applicability of the results obtained in §§2 and 3 cannot be resolved within the framework of the linearized theory. There are two ways to check the range of applicability of the theory when perturbations seem not to be small. The first is to compare the results with experimental data. This is done in figure 3, where we use experimental data obtained under well-defined conditions (such data are scarce), and show that the analytical solution is sufficiently accurate even for relatively large perturbations. One cannot, however, exclude the possibility that the close agreement for one experiment may be fortuitous. Therefore, in principle, further comparison with experimental data is desirable. (One more example, but, only a qualitative one, will be given below for the case of collapse.)

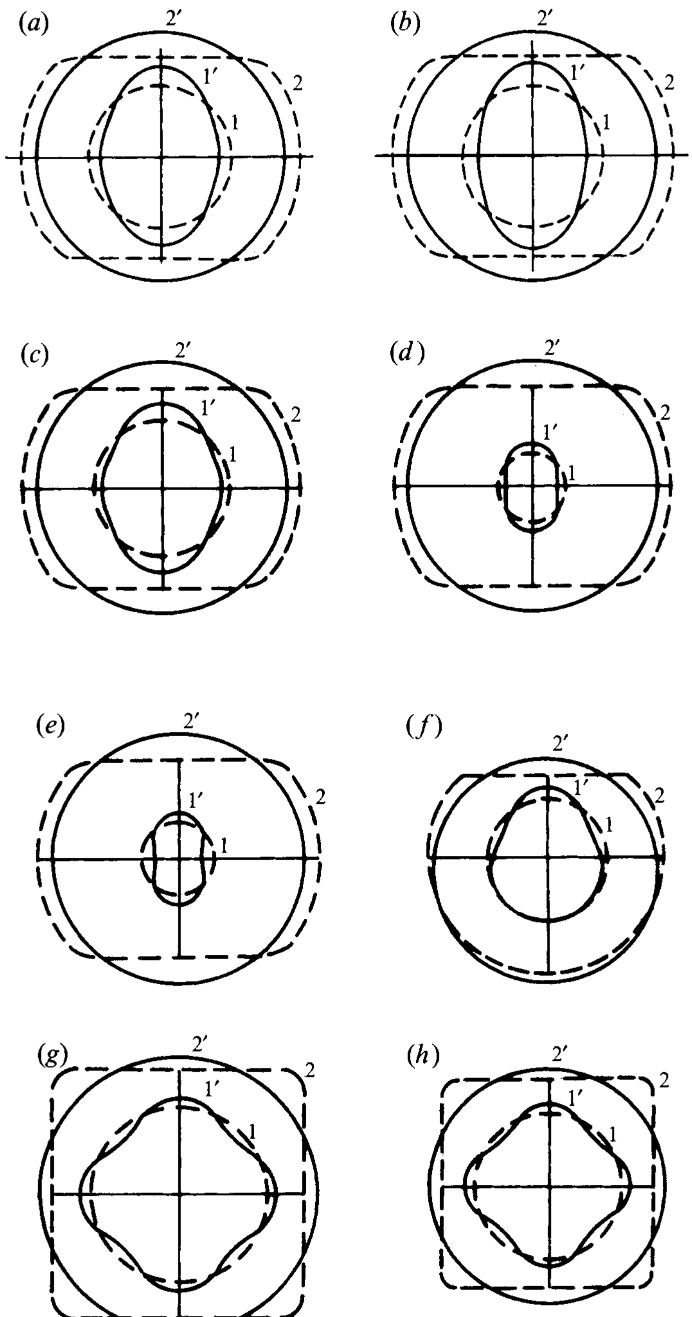

FIGURE 4(a–h). For caption see facing page.

The second way to check the range of applicability of the theory is to develop a fully numerical, large-deformation calculation (e.g. via finite-element methods) and compare its results both to experiment and to the linearized theory of the present work. However, to the best of our knowledge, such a numerical problem still awaits solution. Moreover, for large ellipticities of the cladding or outer matrix (the most doubtful case in the analytical solution) finite-element methods raise huge difficulties because of the

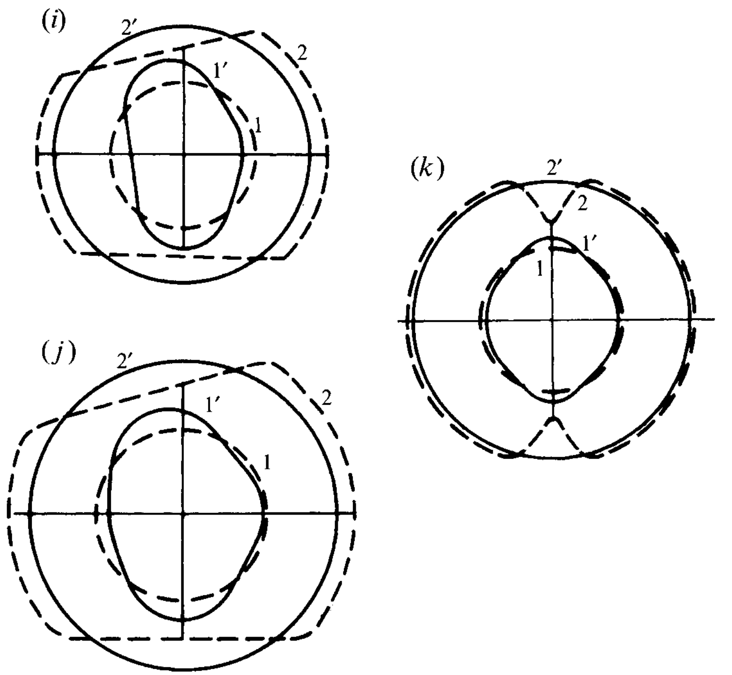

FIGURE 4. Calculated shapes of two-layer preforms for various initial cross-sections of the outer matrix. The dashed curves 1 and 2 show the configurations of the boundaries of the cladding and outer matrix at the initial moment, and the solid curves 1′ and 2′ show these boundaries at the end of the process at steady state. The parameters corresponding to *a–k* are given in table 1.

Figure	γ	μ_1/μ_2	Figure	γ	μ_1/μ_2
4(*a*)	2	1	4(*f*)	2	1
4(*b*)	2	0.2	4(*g*)	2	1
4(*c*)	2	2	4(*h*)	2	0.2
4(*d*)	4	1	4(*i*)	2	0.2
4(*e*)	4	0.2	4*j*)	2	2
			4(*k*)	2	0.2

TABLE 1. Values of the parameters corresponding to figures 4(*a*)–4(*k*). $\alpha_1/\alpha_2 = 0$

high aspect ratio of the elements which, in turn, affects the time step. Thus, one could be also suspicious of the accuracy of such a numerical solution for a cladding or outer matrix with large ellipticity. In any case, the present analytical solution yields a necessary test for any numerical method.

Yarin (1990) found the analytical solution of the thermoelastic problem corresponding to a hard polarization-maintaining preform (or fibre) of the type which results from the polishing or collapse methods considered in the present work. He linearized the boundary conditions of the thermoelastic problem similarly to the present work. Bernat & Yarin (1992) compared this solution with the numerical large-deformation solution of the thermoelastic problem obtained by means of the finite-element method, and agreement was fairly good up to an ellipticity (semi-axes ratio) of 2 (they use the reciprocal value of 0.5). In the absence of a numerical large-deformation solution of the present problem, it is believed that an ellipticity of about 2 represents the range of applicability of the present solution also, since its inaccuracy is similar to that of Yarin (1990). This, in a sense, supports the data shown in figure 4 and (together with the comparison with experiment discussed above) indicates that the present analytical solution can be sufficiently accurate far beyond a linear approximation.

In figure 4 and table 1 it is seen that a fivefold and a tenfold increase in the ratio μ_1/μ_2 at fixed values of γ and $\alpha_1/\alpha_2 = 0$ had only a very slight effect on the results.

In the case of $\gamma = 4$, the results (figures 4*d* and 4*e*) show that the final form of the cladding becomes similar to that of a bow-tie. In optoelectronic applications a bow-tie form of the cladding boundary is preferable because it provides higher birefringence.

When the interfacial tension is negligible, $\alpha_1/\alpha_2 = 0$, the cladding boundary asymptotically approaches a final non-circular form (shown in figures 3 and 4), whereas the outer boundary of the outer matrix tends asymptotically to a circle under the action of surface tension.

We also performed the calculations with non-zero interfacial tension and values of γ and μ_1/μ_2 similar to those shown in table 1.

For $\alpha_1/\alpha_2 = 0.1$, two characteristic timescales of the process can be distinguished. The first is of the order of the timescale based on the surface tension, $\mu_2 R_2/\alpha_2$. In this timescale the flow development at $\alpha_1/\alpha_2 = 0.1$ is almost identical with that for $\alpha_1/\alpha_2 = 0$. The most deformed shapes of the cladding boundaries are practically undistinguishable from those shown in figure 4, whereas the outer boundary of the outer matrix acquires a circular shape. Such an intermediate asymptotic form persists for rather a long time. However, in the timescale based on the interfacial tension, $\mu_2 R_2/\alpha_1$, which is ten times longer than $\mu_2 R_2/\alpha_2$ in the given case, these intermediate asymptotic forms of the cladding disappear, since the cladding should return to the trivial equilibrium form with a circular boundary minimizing the interfacial energy. This, indeed, takes place, and the analytical solution obtained describes monotonic evolution of the cladding forms of figure 4 back to a circular shape, which the boundary of the cladding eventually assumes as time increases. During this process, the outer boundary of the outer matrix continues to be virtually circular.

Several calculations have been done at relatively large interfacial tension, $\alpha_1/\alpha_2 = 0.5$, and the values of γ and μ_1/μ_2 shown in table 1. At such a value of α_1/α_2 the intermediate quasi-steady asymptotic form of the cladding, described above, practically disappears (since the timescales $\mu_2 R_2/\alpha_2$ and $\mu_2 R_2/\alpha_1$ are close to each other), the deformation of the inner (cladding) boundary relative to a circle being only very slight throughout the process of rounding-off of the outer boundary. Therefore, such glasses with high interfacial tension are completely inappropriate for use in the polishing method.

All the results above show the solutions of the direct problem when the initial configuration of the outer matrix obtained by polishing is given, in order to predict the final shape of the cladding boundary. The analytical solution obtained in §2, however, may also be used to answer the inverse problem: what should be the shape of the outer matrix after polishing, to arrive at a given shape of the cladding boundary?

Bearing in mind that in optoelectronic applications a bow-tie shape of cladding is preferable, we predict the initial shape of the outer matrix in a two-layer system, which allows us to arrive at the final configuration of the cladding, for example, in the form of the ovals of Cassini

$$(x^2+y^2)^2-2c^2(x^2-y^2) = a^4-c^4. \tag{4.1}$$

Here the Cartesian coordinates are those of figure 1 and the constants a and c satisfy the inequality $c < a < c\sqrt{2}$ (the only condition under which the ovals resemble a bow-tie).

The area of oval A is equal to the area of an equivalent unperturbed circle, which yields the radius of the latter:

$$A = 2a^2 E\left(\frac{c^2}{a^2}\right) = \pi R_1^2, \quad E\left(\frac{c^2}{a^2}\right) = \int_0^\pi \left(1 - \frac{c^4}{a^4}\sin^2\theta\right)^{1/2} d\theta. \qquad (4.2a, b)$$

Knowing R_1 from (4.2a) we can represent the oval (4.1) as a perturbation of the circle of radius R_1 in the form of (2.2). As a result the perturbation of this circle is given by the expression

$$\zeta_1 = \left[\frac{\pi}{2E(\beta^{-2})}\right]^{1/2} \frac{1}{\beta}[\cos 2\varphi + (\cos^2 2\varphi + \beta^4 - 1)^{1/2}]^{1/2} - 1, \qquad (4.3a)$$

$$\beta = a/c, \quad 1 < \beta < \surd 2. \qquad (4.3b, c)$$

The expression for ζ_1 is used to find the Fourier coefficients a_{n1f} and b_{n1f} corresponding to the final boundary of the oval cladding:

$$a_{n1f} = \frac{1}{\pi}\int_0^{2\pi} \zeta_1(\varphi)\sin n\varphi \, d\varphi, \quad b_{n1f} = \frac{1}{\pi}\int_0^{2\pi} \zeta_1(\varphi)\cos n\varphi \, d\varphi, \quad \forall n. \qquad (4.4a, b)$$

When the interfacial tension is zero, we have from (2.20) and the complementary expression for a_{n1} the following:

$$a_{n1} = a_{n10} + a_{n20}\frac{l_{11}}{l_{21}}[\exp(l_{21} t) - 1], \quad b_{n1} = b_{n10} + b_{n20}\frac{l_{11}}{l_{21}}[\exp(l_{21} t) - 1], \quad n \geqslant 2. \qquad (4.5a, b)$$

Taking $t = t_p$, where t_p is the duration of the process, we arrive from (4.5) at the expressions for the Fourier coefficients of the initial shape of the outer boundary:

$$a_{n20} = \frac{a_{n1f} l_{21}}{l_{11}[\exp(l_{21} t_p) - 1]}, \quad b_{n20} = \frac{b_{n1f} l_{21}}{l_{11}[\exp(l_{21} t_p) - 1]}, \quad n \geqslant 2 \qquad (4.6a, b)$$

(the initial cladding boundary is circular and thus $a_{n10} = b_{n10} = 0$).

Since $l_{21} < 0$, for a sufficiently large t_p we obtain

$$a_{n20} = -a_{n1f}\frac{l_{21}}{l_{11}}, \quad b_{n20} = -b_{n1f}\frac{l_{21}}{l_{11}}, \quad n \geqslant 2. \qquad (4.7a, b)$$

The Fourier coefficients corresponding to the polishing shape of the outer matrix, which in turn leads to the bow-tie shape of the cladding boundary, are thus given by (4.7).

The results for the inverse problem are shown in figure 5 corresponding to $\gamma = 2$, $\mu_1/\mu_2 = 0.2$, $\alpha_1/\alpha_2 = 0$ and $\beta = 1.1$. The prescribed value of β determines the required cladding shape.

We realize clearly that the boundary shape 2 in figure 5 is a rather large perturbation of a circle. The ellipticity of this curve is, however, close to 2, which fits the borderline of the range of applicability of the linearized theory, as was discussed above. Therefore, we hope that the data in figure 5 are a valid approximation of a nonlinear solution, which should be checked in future by solving numerically the corresponding direct problem with 1 and 2 of figure 5 as the initial cladding and outer matrix forms.

Note that such inverse problems are characteristic of engineering (Shercliff 1981). Computers are practically useless in solving such problems. Therefore, even an

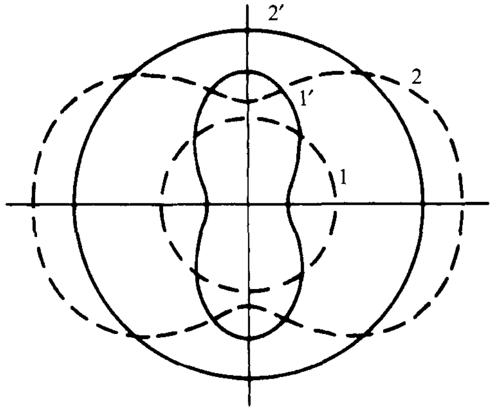

FIGURE 5. Solution of the inverse problem. Predicted initial shape of the outer boundary (curve 2) leading to the final shape of the cladding boundary (curve 1′) in the form of the oval of Cassini with $\beta = 1.1$. The dashed curves 1 and 2 show the initial configurations of the boundaries, and the solid curves 1′ and 2′ show the final ones.

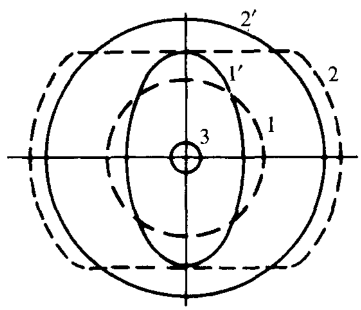

FIGURE 6. Three-layer preform. The dashed curves 1 and 2 show the shapes of the boundaries of the cladding and outer matrix at the initial moment. The solid curves 1′ and 2′ show these boundaries at the end of the process in the steady state. Circle 3 shows the core boundary. $\gamma_0 = 0.2$, $\gamma = 2$, $\mu_1/\mu_2 = 0.2$, $\alpha_1/\alpha_2 = 0$.

γ_0	$\lvert b_{21f}\rvert$
0.1	0.2823
0.2	0.2776
0.3	0.2683
0.4	0.2523
0.5	0.2260

TABLE 2. The effect of the solid core size on the final shape of the cladding for three-layer preforms

approximate analytical solution, like that of figure 5, might be very instructive and helpful in this case.

Consider now three-layer preforms. An example of the direct problem corresponding to $\gamma_0 = 0.2$, $\gamma = 2$, $\mu_1/\mu_2 = 0.2$ and $\alpha_1/\alpha_2 = 0$ is shown in figure 6. The calculated final shape of the cladding (curve 1′), corresponding to the initial polishing of the outer matrix, is close to that of an ellipse. The effect of the solid core size on the final shape of the cladding is illustrated in table 2. There we show the second Fourier coefficient of the cladding boundary $b_{21f}(= b_{21}$ at $t = \infty)$ as a function of γ_0. (This coefficient is

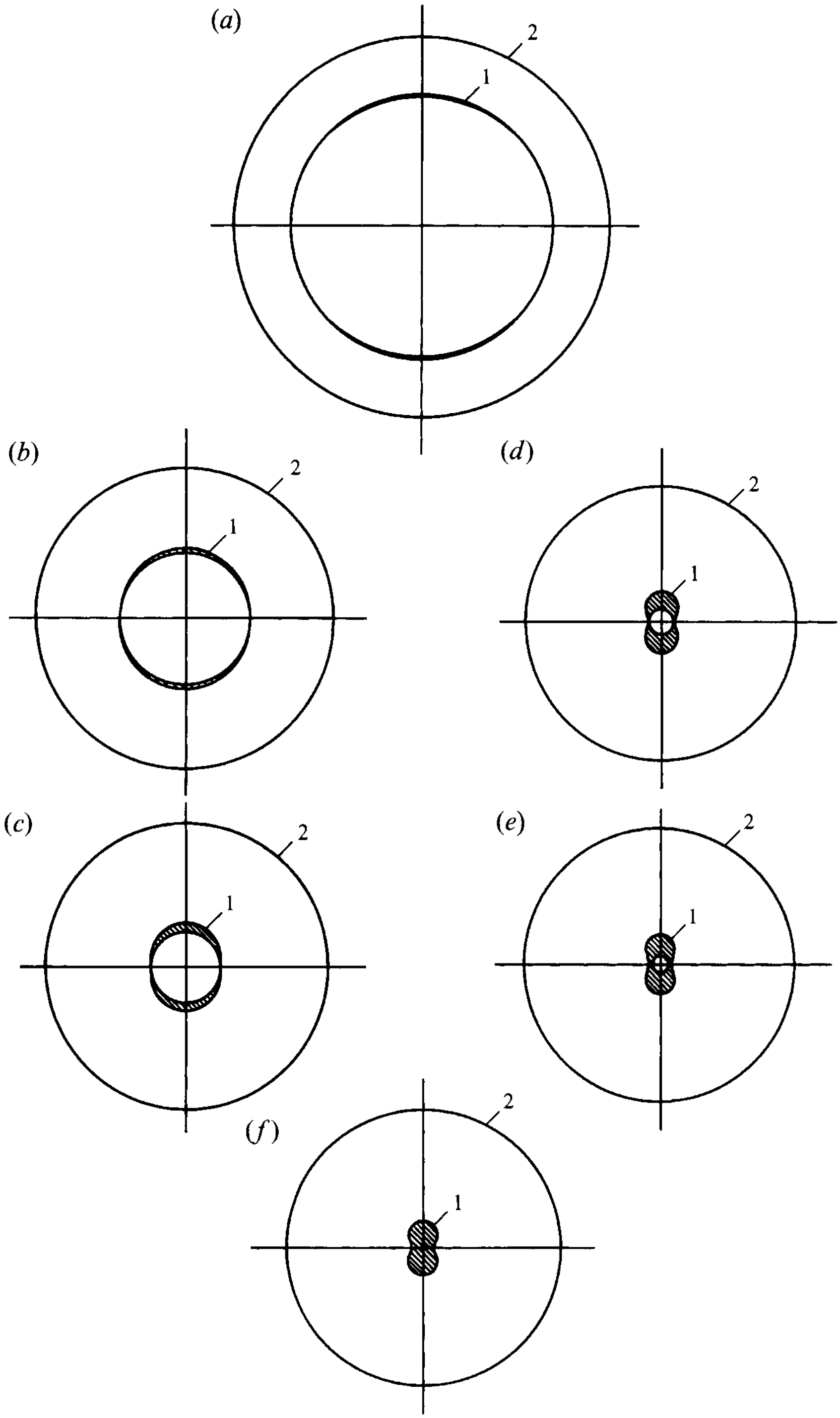

FIGURE 7. The time evolution of the collapse process at various scaled times for the surface tension ratios $\bar{\alpha}_0 = 1$, $\bar{\alpha}_1 = 0$ and the viscosity ratio $\bar{\mu}_1 = 1$ (curves 1: deposited region, 2: substrate tube). (*a*) $\bar{t} = 0$ (the initial shapes of the boundaries; (*b*) $\bar{t} = 0.3$; (*c*) $\bar{t} = 0.5$; (*d*) $\bar{t} = 0.7$; (*e*) $\bar{t} = 0.75$; (*f*) $\bar{t} = 0.827$ (the final state).

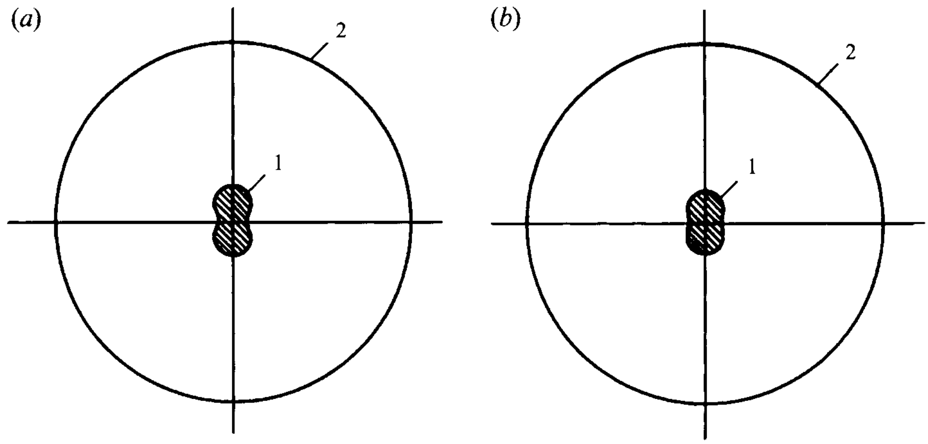

FIGURE 8. The final states of the collapse for various surface tension ratios $\bar{\alpha}_1$; $\bar{\alpha}_0 = 1$, $\bar{\mu}_1 = 1$, the initial geometry is the same as in figure 7(*a*) (curves 1: deposited region, 2: substrate tube). (*a*) $\bar{\alpha} = 0.1$; (*b*) $\bar{\alpha}_1 = 1$.

related to the ellipticity.) The coefficient $b_{21f}(<0)$ is the one that determines the birefringence of the fibre (Yarin 1990; Bernat & Yarin 1992) and its value (as well as the birefringence) decreases as the core radius increases.

4.2. *Method of surface-tension-driven collapse*

The non-symmetrical modified chemical vapour deposition (N-MCVD) process, with the subsequent surface-tension-driven collapse, makes it possible to fabricate preforms with bow-tie shaped claddings (see the photograph in figure 6 in Doupovec & Yarin 1991). In this case the boundaries Γ_1 and Γ_2 in figure 2 may be taken approximately as circles, and the interface Γ_0 as an ellipse with a semi-axes ratio $\delta = c_1/c_2$ satisfying the inequality

$$1 \leqslant \delta \leqslant (\gamma_1/\gamma_*)^2 \tag{4.8}$$

(see (3.9*d*, *e*)). Here we suppose that the radius of the unperturbed circle corresponding to the boundary Γ_0 is equal to $R_{00} = (c_1 c_2)^{1/2}$, which means that the area of this circle is equal to that of the ellipse.

The initial perturbations of the boundaries corresponding to (3.4) are given by

$$\zeta_0 = -1 + (\delta \sin^2\varphi + \delta^{-1}\cos^2\varphi)^{-1/2}, \quad \zeta_1 = \zeta_2 = 0. \tag{4.9a, b}$$

Expression (4.9*a*) describes an elliptical perturbation of the circle of radius R_{00}.

In the calculations we take the following values of the geometrical parameters:

$$\gamma_1 = 1.457, \gamma_* = 1.440, \quad \delta = (\gamma_1/\gamma_*)^2 = 1.023, \tag{4.10a–c}$$

which means that the elliptical boundary Γ_0 at the major axis practically touches Γ_1 (see figure 7*a*).

The time evolution of the surface-tension-driven collapse process is shown in figure 7. The resulting bow-tie-like shape (figure 7*f*) is in qualitative agreement with the one found experimentally (figure 6 in Doupovec & Yarin 1991). Unfortunately, in this experiment the exact parameters of the deposited layer are unknown, which does not allow us to make a quantitative check of the theory in this case.

The final shapes of the surface-tension-driven collapse for the same initial condition as in figure 7 but for different values of $\bar{\alpha}_1$ and $\bar{\mu}_1$ are shown in figures 8 and 9, respectively. Variation in $\bar{\alpha}_1$, as well as in $\bar{\mu}_1$, does not change the fact that a bow-tie-like shape of the cladding appears, as is seen in figures 8 and 9.

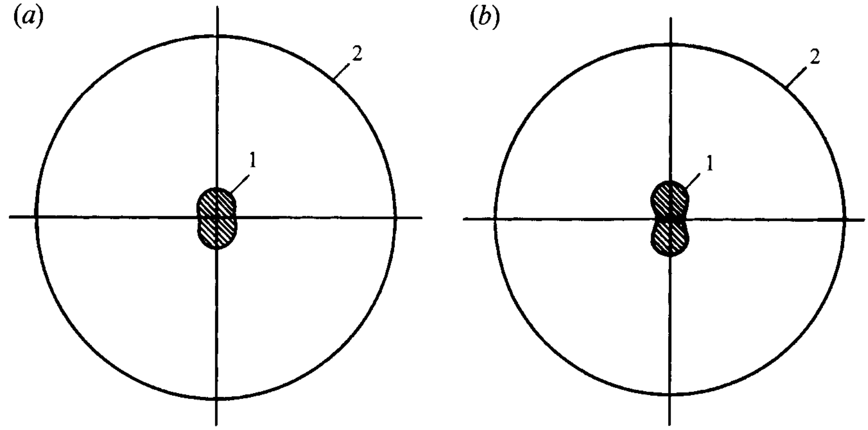

FIGURE 9. The final states of the collapse for various viscosity ratios $\bar{\mu}_1$; $\bar{\alpha}_0 = 1$, $\bar{\alpha}_1 = 0$, the initial geometry is the same as in figure 7(*a*) (curves 1: deposited region, 2: substrate tube). (*a*) $\bar{\mu}_1 = 0.1$; (*b*) $\bar{\mu}_1 = 10$.

5. Conclusion

We obtained the analytical solutions for two hydrodynamic problems related to formation of preforms for drawing of polarization-maintaining optical fibres. In both cases (the polishing method and the collapse method) formation of the desired internal structure of the preform proceeds under the action of the surface tension of softened glass. Both cases are described by the inertialess Stokes equations. The boundaries are considered as perturbations of the appropriate circles and the boundary conditions are linearized.

The solutions obtained allow us to predict the final shape of the cladding boundary for a given initial shape of the outer matrix (in the polishing method) or coating (for the collapse method). These represent the solution of the direct problem. The analytical result allows us also to solve the inverse problem and predict the initial shape of the outer matrix needed to arrive at a given shape of the cladding. The results thus obtained agree fairly well with the experimental data.

In Yarin (1990) the linearized analytical solution of the thermoelastic problem corresponding to a hard polarization-maintaining preform (or fibre) was found. In Bernat & Yarin (1992) the corresponding numerical large-deformation solution was obtained. Therefore, the field of thermoelastic stresses, as well as the birefringence (related to the stress by the stress-optical law), can be readily calculated analytically if the shape of the cladding boundary is known. The present work yields such information and thus, combined with the above thermoelastic solutions, makes it possible to predict analytically the birefringence resulting from initial polishing of the outer matrix, as well as from the shape of the deposited coating in the method of collapse.

The following conclusions might provide some guidance for the designer of polarization-maintaining optical fibres.

(i) A bow-tie-like form of the cladding boundary may be achieved by simple straight polishing of the outer matrix at a relatively large value of $\gamma = 4$ (figures 4*d* and 4*e*).

(ii) Simple straight polishing of the outer matrix yields higher ellipticity of the cladding compared to that which may be achieved at even deeper narrow wedge polishing (cf. figures 4*b* and 4*k*).

(iii) The results of solution of the inverse problem indicate that bow-tie features of the cladding boundary can be strengthened by a small perturbation of simple straight polishing (figure 5).

(iv) The duration of the collapse (or heat treatment in the polishing method) needed to achieve the most deformed cladding form in the case of small non-zero interfacial tension ($\alpha_1/\alpha_2 \sim 0.1$) is of the order of $\mu_2 R_{20}/\alpha_2$.

(v) Glass pairs with relatively high interfacial tension are completely inappropriate for use in the polishing method. They are also less effective in the collapse method.

The author acknowledges fruitful discussions with J. Doupovec, V. M. Entov and Yu. K. Chamorovskii as well as the help of V. Bernat in graphical representation of the collapse patterns. The author is a recipient of the Guastalla Fellowship established by Fondation Rashi, the Planning and Grants Committee of the Council of Higher Education, Israel Academy of Sciences and Humanities. He is also indebted to the Institute of Physics, Slovak Academy of Sciences in Bratislava, for their hospitality in 1989 and 1990.

Appendix A

$$\gamma_0 = R_0/R_1 \leqslant 1, \quad \gamma = R_2/R_1 \geqslant 1, \tag{A 1a, b}$$

$$G_n(\gamma) = (1-\gamma^{2-2n}-\gamma^2+\gamma^{-2n})^{-1}, \tag{A 1c}$$

$$S_1 = (\mu_1/\mu_2)\{(-2n-4+2n^2)+[n(-2n^2-2n)\gamma_0^{2n+2}-(n+1)(-2n+4-2n^2)\gamma_0^{2n}]\}, \tag{A 1d}$$

$$S_2 = (\mu_1/\mu_2)\{(2n^2-2n)+[(n-1)(-2n^2-2n)\gamma_0^{2n}-n(-2n+4-2n^2)\gamma_0^{2n-2}]\}, \tag{A 1e}$$

$$S_3 = G_n(\gamma)n^{-1}[\gamma^{-2n}(-4-2n+2n^2)-\gamma^{2-2n}(-2n+2n^2)+\gamma^2(2n+2n^2) +4-2n-2n^2], \tag{A 1f}$$

$$S_4 = G_n(\gamma)2n^{-1}(\gamma^{2-3n}-2n\gamma^{2-n}+2n\gamma^{-n}+2n^3\gamma^{2-n}-n^3\gamma^{-n}-n^3\gamma^{4-n}-\gamma^{n+2}), \tag{A 1g}$$

$$S_5 = -G_n(\gamma)\frac{\alpha_2}{R_2\mu_2}(\gamma^{2-3n}-2\gamma^{-n}+n^2\gamma^{-n}-n^2\gamma^{4-n}+\gamma^{n+2}), \tag{A 1h}$$

$$S_6 = \frac{\alpha_1}{\alpha_2}\frac{\alpha_2}{\mu_2 R_2}\gamma(1-n^2), \tag{A 1i}$$

$$S_7 = (\mu_1/\mu_2)\{(-2n^2-2n)+[n(-2n^2-2n)\gamma_0^{2n+2}-(n+1)(-2n^2+2n)\gamma_0^{2n}]\}, \tag{A 1j}$$

$$S_8 = (\mu_1/\mu_2)\{(-2n^2+2n)+[(n-1)(-2n^2-2n)\gamma_0^{2n}-n(-2n^2+2n)\gamma_0^{2n-2}]\}, \tag{A 1k}$$

$$S_9 = G_n(\gamma)n^{-1}[2n-2n^2+\gamma^{2-2n}(-2n+2n^2)-\gamma^{-2n}(2n^2+2n)+\gamma^2(2n^2+2n)], \tag{A 1l}$$

$$S_{10} = G_n(\gamma)2n^{-1}(n\gamma^{2-3n}+n^2\gamma^{-n}-n^2\gamma^{4-n}-n\gamma^{n+2}), \tag{A 1m}$$

$$S_{11} = -G_n(\gamma)\frac{\alpha_2}{R_2\mu_2}(n\gamma^{2-3n}-n\gamma^{-n}-n\gamma^{4-n}+n\gamma^{n+2}), \tag{A 1n}$$

$$S_{12} = G_n(\gamma)n^{-1}[(n+2)\gamma^{-2n}-n\gamma^{2-2n}+n\gamma^2-n+2], \tag{A 1o}$$

$$S_{13} = G_n(\gamma)n^{-1}(2n^2\gamma^{2-n}-n^2\gamma^{-n}-\gamma^{2-3n}-2\gamma^{2-n}-n^2\gamma^{4-n}-\gamma^{n+2}), \tag{A 1p}$$

$$S_{14} = G_n(\gamma)\frac{\alpha_2}{2R_2\mu_2}(-n\gamma^{-n}+\gamma^{2-3n}+n\gamma^{4-n}-\gamma^{n+2}), \tag{A 1q}$$

$$S_{15} = (n+2)+[-n^2\gamma_0^{2n+2}-(n+1)(-n+2)\gamma_0^{2n}], \tag{A 1r}$$

$$S_{16} = n+[-n(n-1)\gamma_0^{2n}-n(-n+2)\gamma_0^{2n-2}], \tag{A 1s}$$

$$S_{17} = 1+[n\gamma_0^{2n+2}-(n+1)\gamma_0^{2n}], \tag{A 1t}$$

$$S_{18} = 1+[(n-1)\gamma_0^{2n}-n\gamma_0^{2n-2}]. \tag{A 1u}$$

In addition,

$$k_1 = (S_{15}S_{18}-S_{16}S_{17})(S_3S_8-S_2S_9)-[S_{18}S_{12}-(S_{16}/n)](S_1S_8-S_2S_7), \quad \text{(A 2}a\text{)}$$

$$k_2 = (S_{15}S_{18}-S_{16}S_{17})(S_4S_8-S_2S_{10})-S_{18}S_{13}(S_1S_8-S_2S_7), \quad \text{(A 2}b\text{)}$$

$$k_3 = (S_{15}S_{18}-S_{16}S_{17})(S_5S_8-S_2S_{11})-S_{18}S_{14}(S_1S_8-S_2S_7), \quad \text{(A 2}c\text{)}$$

$$k_4 = (S_{15}S_{18}-S_{16}S_{17})S_6S_8, \quad \text{(A 2}d\text{)}$$

$$k_5 = (S_{15}S_{18}-S_{16}S_{17})(S_1S_9-S_3S_7)-[(S_{15}/n)-S_{17}S_{12}](S_1S_8-S_2S_7), \quad \text{(A 2}e\text{)}$$

$$k_6 = (S_{15}S_{18}-S_{16}S_{17})(S_1S_{10}-S_4S_7)+S_{17}S_{13}(S_1S_8-S_2S_7), \quad \text{(A 2}f\text{)}$$

$$k_7 = (S_{15}S_{18}-S_{16}S_{17})(S_1S_{11}-S_5S_7)+S_{17}S_{14}(S_1S_8-S_2S_7), \quad \text{(A 2}g\text{)}$$

$$k_8 = -(S_{15}S_{18}-S_{16}S_{17})S_6S_7. \quad \text{(A 2}h\text{)}$$

Appendix B

$$\Phi = \frac{1}{2}\left\{\left[-\frac{1}{\bar{R}_2^3}-\frac{\gamma_*^3\bar{\alpha}_1}{\bar{R}_1^3}-\frac{\gamma_1^3\bar{\alpha}_0}{\bar{R}_0^3}\right]\left[\bar{\mu}_1\left(\frac{\gamma_*^2}{\bar{R}_1^2}-\frac{\gamma_1^2}{\bar{R}_0^2}\right)+\left(\frac{1}{\bar{R}_2^2}-\frac{\gamma_*^2}{\bar{R}_1^2}\right)\right]-\left[\frac{1}{\bar{R}_2}+\frac{\gamma_*\bar{\alpha}_1}{\bar{R}_1}+\frac{\gamma_1\bar{\alpha}_0}{\bar{R}_0}\right]\right.$$
$$\left.\times\left[2\bar{\mu}_1\left(-\frac{\gamma_*^4}{\bar{R}_1^4}+\frac{\gamma_1^4}{\bar{R}_0^4}\right)+2\left(-\frac{1}{\bar{R}_2^4}+\frac{\gamma_*^4}{\bar{R}_1^4}\right)\right]\right\}\Big/\left[\bar{\mu}_1\left(\frac{\gamma_*^2}{\bar{R}_1^2}-\frac{\gamma_1^2}{\bar{R}_0^2}\right)+\left(\frac{1}{\bar{R}_2^2}-\frac{\gamma_*^2}{\bar{R}_1^2}\right)\right]^2, \quad \text{(B 1}a\text{)}$$

$$\Phi_0 = \gamma_1^2\frac{\Phi F\bar{R}_0^2-\gamma_1^2F^2}{\bar{R}_0^3}, \quad \Phi_1 = \gamma_*^2\frac{\Phi F\bar{R}_1^2-\gamma_*^2F^2}{\bar{R}_1^3}, \quad \text{(B 1}b, c\text{)}$$

$$\Phi_2 = \frac{\gamma_*}{\gamma_1}\frac{\bar{R}_0}{\bar{R}_1}\frac{\Phi_1\gamma_1^2\gamma_*^{-2}\bar{R}_1-\Phi_0\bar{R}_0}{\gamma_1^2F}\frac{\bar{\mu}_1-1}{\bar{\mu}_1}, \quad \text{(B 1}d\text{)}$$

$$\Phi_3 = \frac{\gamma_*}{\gamma_1}\frac{\bar{R}_0}{\bar{R}_1}\frac{\bar{\mu}_1-1}{\bar{\mu}_1}, \quad \gamma_0 = \frac{\gamma_*}{\gamma_1}\frac{\bar{R}_0}{\bar{R}_1}, \quad \gamma = \gamma_*\frac{\bar{R}_2}{\bar{R}_1}, \quad \text{(B 1}e\text{–}g\text{)}$$

$$Z_1 = \frac{3+\gamma_0^4}{\bar{\mu}_1(1-\gamma_0^4)}-\frac{3\gamma^{-2}+\gamma^2}{-\gamma^2+\gamma^{-2}}+\gamma_0\Phi_3, \quad Z_2 = -\gamma\frac{3+\gamma_0^4}{\bar{\mu}_1(1-\gamma_0^4)}+\frac{2\gamma^{-1}+2\gamma^3}{-\gamma^2+\gamma^{-2}}, \quad \text{(B 1}h, i\text{)}$$

$$Z_3 = \frac{1}{\bar{R}_2}\frac{\mathrm{d}\bar{R}_2}{\mathrm{d}\bar{t}}\left[-\frac{(3+\gamma_0^4)\gamma(2+\ln\gamma)}{\bar{\mu}_1(1-\gamma_0^4)}+\frac{3\gamma^3+5\gamma^{-1}+2\gamma\ln\gamma(\gamma^2+\gamma^{-2})}{-\gamma^2+\gamma^{-2}}\right], \quad \text{(B 1}j\text{)}$$

$$Z_4 = \frac{1}{\bar{R}_1}\frac{\mathrm{d}\bar{R}_1}{\mathrm{d}\bar{t}}\left[\frac{2(3+\gamma_0^4)}{\bar{\mu}_1(1-\gamma_0^4)}+\frac{(\ln\gamma_0-1)(\bar{\mu}_1-1)}{\bar{\mu}_1}-\frac{2(3\gamma^{-2}+\gamma^2)}{-\gamma^2+\gamma^{-2}}\right]+\gamma_0\Phi_2+\frac{2\gamma_0}{\bar{R}_0}\frac{\mathrm{d}\bar{R}_0}{\mathrm{d}\bar{t}}\Phi_3, \quad \text{(B 1}k\text{)}$$

$$Z_5 = \frac{1}{\bar{\mu}_1}-1+\gamma_0\Phi_3, \quad Z_6 = -\frac{\gamma}{\bar{\mu}_1}, \quad Z_7 = -\frac{1}{\bar{\mu}_1}\frac{1}{\bar{R}_2}\frac{\mathrm{d}\bar{R}_2}{\mathrm{d}\bar{t}}\gamma(1+\ln\gamma), \quad \text{(B 1}l\text{–}n\text{)}$$

$$Z_8 = \frac{2}{\bar{\mu}_1\bar{R}_1}\frac{\mathrm{d}\bar{R}_1}{\mathrm{d}\bar{t}}+\frac{\ln\gamma_0}{\bar{R}_1}\frac{\mathrm{d}\bar{R}_1}{\mathrm{d}\bar{t}}\frac{\bar{\mu}_1-1}{\bar{\mu}_1}+\gamma_0\Phi_2+\frac{2\gamma_0}{\bar{R}_0}\frac{\mathrm{d}\bar{R}_0}{\mathrm{d}\bar{t}}\Phi_3-\frac{2}{\bar{R}_1}\frac{\mathrm{d}\bar{R}_1}{\mathrm{d}\bar{t}}. \quad \text{(B 1}o\text{)}$$

Appendix C

$$F_1' = -(k_3 b_{n2}+k_4 b_{n1}+k_4'' b_{n0}), \quad F_2 = -(k_7 b_{n2}+k_8 b_{n1}+k_8'' b_{n0}), \tag{C 1a, b}$$
$$F_3 = -(k_{12} b_{n2}+k_{13} b_{n1}+k_{14} b_{n0}), \tag{C 1c}$$
$$F_4 = k_1 k_6 k_{11}+k_2 k_8' k_9+k_4' k_5 k_{10}-k_9 k_6 k_4'-k_{10} k_8' k_1-k_{11} k_5 k_2, \tag{C 1d}$$
$$S_a = S_1 S_8-S_2 S_7, \quad S_b = S_{15} S_{18}-S_{16} S_{17}, \tag{C 1e, f}$$
$$k_1 = S_b(S_3 S_8-S_2 S_9)-S_a(S_{12} S_{18}-S_{16} S_{19}), \tag{C 1g}$$
$$k_2 = S_b(S_4 S_8-S_2 S_{10})-S_a S_{13} S_{18}, \quad k_3 = S_b(S_5 S_8-S_2 S_{11})-S_a S_{14} S_{18}, \tag{C 1h, i}$$
$$k_4 = S_b(S_6 S_8-S_2 S_{11}')-S_a(S_{14} S_{18}-S_{20}, S_{16}), \tag{C 1j}$$
$$k_4' = S_b(-S_6' S_8+S_2 S_{11}'')+S_a(S_{16}' S_{18}+S_{21} S_{16}), \tag{C 1k}$$
$$k_4'' = S_b(-S_6'' S_8+S_2 S_{11}''')+S_a(S_{16}'' S_{18}+S_{22} S_{16}), \tag{C 1l}$$
$$k_5 = S_b(S_1 S_9-S_7 S_3)-S_a(S_{15} S_{19}-S_{17} S_{12}), \tag{C 1m}$$
$$k_6 = S_b(S_1 S_{10}-S_7 S_4)+S_a S_{17} S_{13}, \quad k_7 = S_b(S_1 S_{11}-S_7 S_5)+S_a S_{17} S_{14}, \tag{C 1n, o}$$
$$k_8 = S_b(S_1 S_{11}'-S_6 S_7)-S_a(S_{15} S_{20}-S_{14}' S_{17}), \tag{C 1p}$$
$$k_8' = S_b(-S_1 S_{11}''+S_6' S_7)-S_a(S_{15} S_{21}+S_{16}' S_{17}), \tag{C 1q}$$
$$k_8'' = S_b(-S_1 S_{11}'''+S_6'' S_7)-S_a(S_{15} S_{22}+S_{16}'' S_{17}), \tag{C 1r}$$
$$k_9 = (S_3 S_8-S_2 S_9+S_1 S_9-S_7 S_3)/S_a, \tag{C 1s}$$
$$k_{10} = (S_4 S_8-S_2 S_{10}+S_1 S_{10}-S_7 S_4)/S_a, \tag{C 1t}$$
$$k_{11} = (-S_6' S_8+S_2 S_{11}''-S_1 S_{11}''+S_7 S_6')/S_a-S_{23}, \tag{C 1u}$$
$$k_{12} = (S_5 S_8-S_2 S_{11}+S_1 S_{11}-S_7 S_5)/S_a, \tag{C 1v}$$
$$k_{13} = (S_6 S_8-S_2 S_{11}'+S_1 S_{11}'-S_7 S_6)/S_a, \tag{C 1w}$$
$$k_{14} = (-S_6'' S_8+S_2 S_{11}'''-S_1 S_{11}'''+S_7 S_6'')/S_a-S_{24}, \tag{C 1x}$$

where

$$S_1 = \bar{\mu}_1[-2n-4+2n^2+(2n^2+2n)\gamma_0^{2n+2}], \tag{C 2a}$$
$$S_2 = \bar{\mu}_1[-2n+2n^2+(2n^2+2n-4)\gamma_0^{2n-2}], \tag{C 2b}$$

$$S_5 = G_n(\gamma)\left\{-\frac{1}{\bar{R}_2}(\gamma^{2-3n}-2\gamma^{-n}+n^2\gamma^{-n}-n^2\gamma^{4-n}+\gamma^{n+2}) + \frac{4}{\bar{R}_2}\frac{\mathrm{d}\bar{R}_2}{\mathrm{d}\bar{t}}\left[\frac{S_4}{2G_n(\gamma)}-\frac{1}{n^2-1}(\gamma^{2-3n}-2\gamma^{-n}+n^2\gamma^{-n}-n^2\gamma^{4-n}+\gamma^{n+2})\right]\right\}, \tag{C 2c}$$

$$S_6 = \bar{\alpha}_1\gamma\frac{1}{\bar{R}_2}(1-n^2)+\frac{4}{\bar{R}_1}\frac{\mathrm{d}\bar{R}_1}{\mathrm{d}\bar{t}}-\frac{4\bar{\mu}_1}{\bar{R}_1}\frac{\mathrm{d}\bar{R}_1}{\mathrm{d}\bar{t}}+\frac{2}{\bar{R}_1}\frac{\mathrm{d}\bar{R}_1}{\mathrm{d}\bar{t}}S_3, \tag{C 2d}$$

$$S_6' = \bar{\mu}_1\left[(-n-1)\gamma_0^{n+2}(-n+1)+\gamma_0^n\frac{n+1}{2n}(-2n+4-2n^2)\right], \tag{C 2e}$$

$$S_6'' = S_6'\frac{2}{\bar{R}_0}\frac{\mathrm{d}\bar{R}_0}{\mathrm{d}\bar{t}}, \tag{C 2f}$$

$$S_7 = -\bar{\mu}_1(2n^2+2n)(1-\gamma_0^{2n+2}), \quad S_8 = \bar{\mu}_1(-2n^2+2n)(1-\gamma_0^{2n-2}), \tag{C 2g, h}$$

$$S_{11} = G_n(\gamma)\left\{-\frac{1}{\bar{R}_2}(n\gamma^{2-3n}-n\gamma^{-n}-n\gamma^{4-n}+n\gamma^{n+2})\right.$$
$$\left.+\frac{4}{\bar{R}_2}\frac{\mathrm{d}\bar{R}_2}{\mathrm{d}\bar{t}}\left[\frac{S_{10}}{2G_n(\gamma)}-\frac{1}{n^2-1}(n\gamma^{2-3n}-n\gamma^{-n}-n\gamma^{4-n}+n\gamma^{n+2})\right]\right\}, \quad (\mathrm{C}\,2i)$$

$$S'_{11} = S_9\frac{2}{\bar{R}_1}\frac{\mathrm{d}\bar{R}_1}{\mathrm{d}\bar{t}}, \quad S''_{11} = \bar{\mu}_1(1-n^2)(\gamma_0^n-\gamma_0^{n+2}), \quad S'''_{11} = S''_{11}\frac{2}{\bar{R}_0}\frac{\mathrm{d}\bar{R}_0}{\mathrm{d}\bar{t}}, \quad (\mathrm{C}\,2j\text{–}l)$$

$$S_{14} = G_n(\gamma)\left\{\frac{1}{2\bar{R}_2}(\gamma^{2-3n}-n\gamma^{-n}+n\gamma^{4-n}-\gamma^{n+2})\right.$$
$$\left.+\frac{1}{\bar{R}_2}\frac{\mathrm{d}\bar{R}_2}{\mathrm{d}\bar{t}}\left[\frac{2S_{13}}{G_n(\gamma)}+\frac{2}{n^2-1}(\gamma^{2-3n}-n\gamma^{-n}+n\gamma^{4-n}-\gamma^{n+2})\right]\right\}, \quad (\mathrm{C}\,2m)$$

$$S'_{14} = S_{12}\frac{2}{\bar{R}_1}\frac{\mathrm{d}\bar{R}_1}{\mathrm{d}\bar{t}}, \quad S_{15} = (n+2)+n\gamma_0^{2n+2}, \quad S_{16} = n-\gamma_0^{2n-2}(-n+2), \quad (C\,2n\text{–}p)$$

$$S'_{16} = -\frac{-n+1}{2}\gamma_0^{n+2}+(-n+2)\frac{n+1}{2n}\gamma_0^n, \quad (\mathrm{C}\,2q)$$

$$S''_{16} = S'_{16}\frac{2}{\bar{R}_0}\frac{\mathrm{d}\bar{R}_0}{\mathrm{d}\bar{t}}, \quad S_{17} = 1-\gamma_0^{2n+2}, \quad S_{18} = 1-\gamma_0^{2n-2}, \quad S_{19} = 1/n, \quad (C\,2r\text{–}u)$$

$$S_{20} = \frac{2}{n\bar{R}_1}\frac{\mathrm{d}\bar{R}_1}{\mathrm{d}\bar{t}}, \quad S_{21} = -\frac{-n+1}{2n}\gamma_0^{n+2}-\frac{n+1}{2n}\gamma_0^n, \quad (\mathrm{C}\,2v,\,w)$$

$$S_{22} = S_{21}\frac{2}{\bar{R}_0}\frac{\mathrm{d}\bar{R}_0}{\mathrm{d}\bar{t}}, \quad S_{23} = \frac{1}{2n}, \quad (\mathrm{C}\,2x,\,y)$$

$$S_{24} = \frac{n^2-n-1}{n(n^2-1)}\frac{1}{\bar{R}_0}\frac{\mathrm{d}\bar{R}_0}{\mathrm{d}\bar{t}}+\frac{\bar{\alpha}_0\gamma_1}{4\bar{\mu}_1\bar{R}_0}. \quad (\mathrm{C}\,2z)$$

Note that $G_n(\gamma)$, S_3, S_4, S_9, S_{10}, S_{12}, S_{13} are given by (A 1*c*, *f*, *g*, *l*, *m*, *o*, *p*), respectively.

REFERENCES

BEJAN, A. 1993 *Heat Transfer*. Wiley.

BERNAT, V. & YARIN, A. L. 1992 Analytical solution for stresses and material birefringence in optical fibers with non-circular cladding. *J. Lightwave Technol.* **10**, 413.

DAS, S. K. & GANDHI, K. S. 1986 A model for thermal collapse of tubes: applications to optical glass fibers. *Chem. Engng Sci.* **41**, 73.

DOREMUS, R. H. 1973 *Glass Science*. Wiley.

DOUPOVEC, J. & YARIN, A. L. 1991 Non-symmetrical modified chemical vapor deposition (N-MCVD) process. *J. Lightwave Technol.* **9**, 695.

FORSYTHE, G. E., MALCOLM, M. A. & MOLER, C. B. 1977 *Computer Methods for Mathematical Computation*. Prentice-Hall.

GEYLING, F. T., WALKER, K. L. & CSENTITS, R. 1983 The viscous collapse of thick-walled tubes. In *Proc. ASME Appl. Mech., Bioengng and Fluids Engng Conf., Houston, TX, Paper* 83-APM-27.

GRIGOR'YANTS, V. V., ENTOV, V. M., IVANOV, G. E., CHAMOROVSKII, YU. K. & YARIN, A. L. 1989 Formation of two-layer preforms for optical-fibers with shaped cores. *Sov. Phys. Dokl.* **34**, 368.

HAPPEL, J. & BRENNER, H. 1965 *Low Reynolds Number Hydrodynamics*. Prentice-Hall.

KAMINOW, I. P. 1981 Polarization – maintaining fibers. In *Proc. First Intl Conf. MIT*, p. 169.

KAMINOW, I. P., PLEIBEL, W., RAMASWAMY, V. & STOLEN, R. H. 1979 U.K. Patent No. 2012983 A.

LEWIS, J. A. 1977 The collapse of a viscous tube. *J. Fluid Mech.* **81**, 129.

MOREY, G. W. 1938, 1954 *The Properties of Glass*. Reinhold.

OH, S. M. 1979 Cooling rates of optical fibers during drawing. *Ceramic Bull.* **58**, 1108.

PAEK, U. C. & RUNK, R. B. 1978 Physical behavior of the neck-down region during furnace drawing of silica fibers. *J. Appl. Phys.* **49**, 4417.

SCHOLZE, H. 1991 *Glass: Nature, Structure and Properties*. Springer.

SHERCLIFF, J. A. 1981 Reflections of a new editor. *J. Fluid Mech.* **106**, 349.

YARIN, A. L. 1990 Hydrodynamic analysis of the process of making three-layer optical fibers and calculation of the field of elastic stresses and birefringence. *J. Appl. Mech. Tech. Phys.* **31**, 361.

YARIN, A. L. 1993 *Free Liquid Jets and Films: Hydrodynamics and Rheology*. Longman.

ZIABICKI, A. 1976 *Fundamentals of Fibre Formation*. Wiley.